U.S. Department of Commerce
National Oceanic and Atmospheric Administration
National Weather Service
National Centers for Environmental Prediction
5830 University Research Court
College Park, MD 20740-3818

Office Note 512
https://doi.org/10.25923/cryn-tp50

Solar and Thermal Infrared Radiation Transfer Schemes in the NCEP Global Forecast System (GFS)

Qingfu Liu and Fanglin Yang

NOAA/NWS/NCEP Environmental Modeling Center

College Park, Maryland

March 2023

E-mail: Qingfu.Liu@noaa.gov

Table of Contents

1. Introduction

Radiative transfer in the Earth's atmosphere plays a major role in the energy budget of the weather and climate system. Roughly 70% of the incoming solar radiation is absorbed by the earth-atmosphere-ocean system, and the remaining part is reflected back to space. The land and ocean surfaces absorb ~ 44% of the incoming solar energy, and the atmosphere absorbs ~ 26%. To maintain an equilibrium energy state, the land-atmosphere-ocean system emits thermal infrared radiation. Over a sufficiently long period of time, the absorbed solar energy is balanced by the outgoing thermal infrared radiation emitted by the land-atmosphere-ocean system, so the Earth's temperature is relatively stable.

The incoming solar radiation is unevenly distributed over the planet Earth. The Sun heats the tropics more compared to the middle to high latitudes. Those excessive radiative energy in the tropics need to be redistributed to middle to high latitudes by the atmosphere and ocean. To even out the radiative imbalances, the atmosphere and ocean work non-stop through the weather systems and ocean circulation to transport energy from tropics to middle and high latitudes. Therefore to understand and predict the weather and climate of the land-atmosphere-ocean system, we need to accurately calculate the radiative transfer in the atmosphere.

Modeling the radiative processes are among the most complex and computationally intensive parts of all model physics. It is difficult to build a parameterization that is both fast and accurate to calculate the radiative transfer. For computational efficiency reasons, atmospheric general circulation models (GCM) generally use broadband parameterization to calculate radiative transfer. Numerous simplifications and approximations are made in these parameterizations. The use of the correlated-*k* method appears to be a computationally efficient and accurate approach to calculate radiative transfer in atmosphere models (Goody et al. 1989; Fu and Liou 1992). In the correlated-*k* method, absorption coefficients as a function of wavenumber are reordered monotonically to create a k-distribution, therefore allowing spectral elements with similar opacities to be grouped together and treated as a single monochromatic element. This technique reduces the number of needed individual radiation calculations by ~10^5 relative to line-by-line calculations, thereby allowing a dramatic increase in the computation speed while maintaining an acceptable level of accuracy for climate and weather simulations (Mlawer et al. 2016).

The GFS radiation scheme is intended to provide the total radiative flux at any given location. These calculations provide both the total radiative flux at the ground surface, which is needed to establish the surface energy budget, and the vertical radiative flux divergence, which is used to calculate the radiative heating and cooling rates of a given atmospheric layer. The magnitude of the terms in the surface energy budget can set the stage for moist deep convection and are crucial to the formation of low-level clouds. In addition, the vertical

radiative flux divergence can produce substantial cooling, particularly at the tops of clouds, which can have strong dynamical and thermal effects on cloud evolution.

A Rapid Radiation Transfer Model for GCM (RRTMG) has become operational in the GFS since 2007. RRTMG (Mlawer, et al., 2016; Mlawer et al., 1997; Mlawer and Clough, 1998) uses a correlated-*k* distribution method and a transmittance lookup table that is linearly scaled by optical depth to achieve high accuracy and efficiency. RRTMG has been validated using the line-by-line radiative transfer model (LBLRTM) (Clough et al. 1992; Clough and Iacono, 1995) for a wide range of clear-sky temperature and moisture profiles. The RRTMG LW algorithm contains 140 unevenly distributed g-points (quadrature points) in 16 broad spectral bands, while the RRTMG SW algorithm includes 112 g-points in 14 bands. In addition to the major atmospheric absorbing gasses of ozone, water vapor, and carbon dioxide, the algorithm also includes various minor absorbing species such as methane, nitrous oxide, oxygen, and in the longwave up to four types of halocarbons (CFCs). To represent statistically the unresolved subgrid cloud variability when dealing with multi layered clouds, a Monte-Carlo Independent Column Approximation (McICA) method is used in the RRTMG radiative transfer. A decorrelation length overlap method is used in both LW and SW radiation calculations. Cloud condensate path and effective radius for water and ice are used for the calculation of cloud-radiative properties.

This technical memorandum is intended to document the radiative transfer scheme used in the current NCEP's models. Sections 2-5 review the fundamentals of radiative transfer calculations for atmospheric model applications. Specifically, section 2 gives the basic equation of the radiative transfer in the plane-parallel atmosphere, section 3 and 4 review the approximations for solar and thermal infrared radiation transfer. Section 5 discusses the radiative flux calculation for partially cloudy sky. Sections 2-5 are very important to understand the GFS radiation scheme. Section 6 introduces the RRTM, RRTMG and RRTMGP radiative transfer models. Section 7 discusses the climate data needed for radiative transfer calculation. Section 8 describes the input variables for the GFS radiative transfer modules. Finally, the GFS radiation scheme FORTRAN code structure is explained in section 9.

2. Basic Equations of Radiative Transfer for Atmospheric Models

The fundamentals of radiative transfer for atmospheric models are reviewed in sections 2-5. Those fundamentals are the key to understanding the GFS radiation packages and RRTMG radiative transfer calculations. The purpose of this section is to present the basic radiative transfer formulas and its discretization in multiple scattering and emitting layered media.

The azimuthally independent equation describing the transfer of monochromatic radiation at wavenumber v through a plane-parallel homogeneous medium is given by (Liou, 2002, Stamnes et al. 1988) (the subscript wavenumber ν is omitted for simplicity of presentation),

$$\mu \frac{dI(\tau,\mu)}{d\tau} = I(\tau,\mu) - S(\tau,\mu) \qquad (2.1)$$

Where $\mu = cos\theta$, θ is the zenith angle, τ is the optical depth, and $S(\tau,\mu)$ is the source function and is given by

$$S(\tau,\mu) = \frac{\omega}{2}\int_{-1}^{1} I(\tau,\mu')P(\mu,\mu')d\mu' + Q(\tau,\mu) \qquad (2.2)$$

where ω is the single scattering albedo, $P(\mu,\mu')$ is the azimuth-independent phase function, and $Q(\tau,\mu)$ is the source term which contains both the direct beam $Q^{(beam)}$ (pseudo-beam) and thermal emission $Q^{(thermal)}$ (in local thermodynamic equilibrium), and is given by (Stamnes et al. 2000),

$$Q(\tau,\mu) = Q^{(beam)}(\tau,\mu) + Q^{(thermal)}(\tau,\mu) \qquad (2.3)$$

and

$$Q^{(beam)}(\tau,\mu) = \frac{\omega}{4\pi}P(\mu,-\mu_0)I_0 e^{-\tau/\mu_0} \qquad (2.4)$$

$$Q^{(thermal)}(\tau,\mu) = (1-\omega)B[\theta(\tau)] \qquad (2.5)$$

where I_0 is the intensity of a 'direct' or parallel beam at top of atmosphere (TOA), and $\mu_0 = cos\theta_0$, θ_0 is the zenith angle of the 'direct' beam, $B(\theta)$ is the Planck Function for substance with temperature θ. Three factors contribute to the source function: multiple scattering of diffuse intensity, single scattering of a 'direct' beam irradiance (flux density) at TOA attenuated to the level τ, and thermal emission of the local medium.

Most of the radiative transfer models ignore either the thermal or the beam source term, some of them allow for both to be present, but take computational shortcuts when one or the other is absent. For solar radiation, $I_0 = F_0$in equation (2.4), where $F_0$is the direct solar irradiance (flux density) at top of atmosphere (TOA). $\mu_0 = cos\theta_0$, θ_0 is the solar zenith angle. $Q^{(thermal)} \approx 0$. For thermal infrared radiation, $I_0 = 0$.

Let β_e, β_s, and β_a denotes the extinction, scattering, and absorption coefficients (in units of per length), respectively, and $\beta_e = \beta_s + \beta_a$, the single scattering albedo is defined as,

$$\omega = \beta_s/\beta_e \tag{2.6a}$$

Or coalbedo,

$$1 - \omega = \beta_a/\beta_e \tag{2.6b}$$

The optical depth of a plane parallel atmosphere from top to z can be expressed as,

$$\tau = \int_z^\infty k_\nu(z')\rho_a(z')dz' \tag{2.7}$$

Where k_ν is the gas absorption coefficient at wavenumber ν, and ρ_a is the density of absorbing glasses.

In the context of the discrete-ordinates method for radiative transfer (Liou 1992), the scattering phase function can be expanded in terms of Legendre polynomials P_l as:

$$P(cos\Theta) = \sum_{l=0}^{N} \omega_l P_l(cos\Theta) \tag{2.8}$$

Where Θ is the scattering angle, and the expansion coefficients ω_l can be determined from the orthogonal property of Legendre polynomials as follows:

$$\omega_l = \frac{2l+1}{2} \int_{-1}^{1} P(cos\Theta)P_l(cos\Theta)d\,cos\Theta \tag{2.9}$$

where $l = 0, 1, \ldots, N$, and the coefficients have the following properties,

$$\omega_0 = 1$$

$$\omega_1/3 = g$$

Where *g* is the asymmetry factor. Using the additional theorem for Legendre polynomials, the azimuth-independent phase function can be written as,

$$P(\mu, \mu') = \sum_{l=0}^{N} \omega_l P_l(\mu) P_l(\mu') \qquad (2.10)$$

Replacing the integral by summation, equation (2.1) may be written as,

$$\mu_i \frac{dI(\tau,\mu_i)}{d\tau} = I(\tau, \mu_i) - \frac{\omega}{2} \sum_{j=-n}^{n} I(\tau, \mu_j) P_l(\mu_i, \mu_j) a_j - \frac{\omega}{4\pi} P(\mu_i, -\mu_0) I_0 e^{-\tau/\mu_0} + (1 - \omega) B[\theta(\tau)] \qquad (2.11)$$

Where $i = \pm 1, \ldots, \pm n$. Each μ_i is called a "stream", and we call this a "2n–stream approximation". It is convenient to draw the μ_j from a Gaussian quadrature point and to have them be mirror symmetric $\mu_{-j} = -\mu_j \ (j \neq 0)$, weight $a_{-j} = a_j$. Using the properties of Legendre polynomials, equation (2.11) can be further simplified and solved for various 2n-stream approximations (Stamnes et al. 2000). When n=1, we have a two-stream approximation, which has been used widely in GCM models for radiative transfer calculation. The two-stream approximation will be discussed in detail in this tech note. When n=2, we have a four-stream approximation, which has been discussed in various text books and literature (Liou, 2002). A discrete ordinate radiative transfer method (DISORT), which uses multi-stream approximation, was developed by Stamnes et al (1988). DISORT for a multi-layered plane-parallel medium has been used by the RRTM_SW, and later was replaced with a much faster two-stream radiative transfer solver.

The monochromatic upward and downward diffuse flux at a given optical depth level, τ, are defined by,

$$F_{dif}^{\pm}(\tau) = 2\pi \int_0^{\pm 1} I(\tau, \mu) \mu d\mu \qquad (2.12)$$

Where the superscripts + and - denote the upward and downward fluxes, respectively.

The direct downward flux at level τ is given by the exponential attenuation of the effective direct-beam contribution at TOA, $\mu_0 I_0$, thus,

$$F^{-}_{dir}(\tau) = \mu_0 I_0 e^{-\tau/\mu_0} \quad (2.13)$$

The total upward and downward fluxes covering the entire spectrum, using the height coordinate, may be written as,

$$F^{+}(z) = \int_0^{\infty} F^{+}_{dif}(\tau) d\lambda \quad (2.14a)$$

$$F^{-}(z) = \int_0^{\infty} (F^{-}_{dif}(\tau) + F^{-}_{dir}(\tau)) d\lambda \quad (2.14b)$$

Thus the net flux is

$$F\ (z) = F^{-}(z) - F^{+}(z) \quad (2.15)$$

The heating rate due to the radiation in the atmosphere is produced by the divergence of the net radiative flux, and is given by

$$\left(\frac{\partial T}{\partial t}\right) = \frac{1}{\rho C_p} \frac{dF\ (z)}{dz} \quad (2.16)$$

Where ρ is the air density and C_p is the specific heat at constant pressure.

The GFS radiation scheme calculates the shortwave and longwave radiative fluxes separately. The methods used in the GFS radiation package will be discussed in detail in the next sections.

3. Solar Radiative Transfer

The spectrum of solar radiation is close to that of a blackbody with a temperature of about 6000 K. The spectrum spans roughly from 0.2 μm to 4 μm, and has its peak energy located at about 0.47 μm. About half of the radiation is in the visible short-wave part of the electromagnetic spectrum (0.3 to 0.7 μm). The other half is mostly in the near-infrared part (> 0.7 μm), with some in the ultraviolet part of the spectrum (< 0.3 μm). In the ultraviolet and visible (UVV) spectral regions ($\lambda < 0.7\mu$), atmospheric ozone is the primary absorber, while water vapor absorption dominates the near infrared (NIR) spectrum region ($\lambda > 0.7\mu$).

Absorptions from other gasses, such as O2 and CO2 also present in the various spectrum locations, but their contributions to atmospheric heating are small.

3.1 Solar Radiative Transfer Approximations

In the Earth's atmosphere, scattering of solar radiation by aerosols and clouds is important, and thermal emission can be neglected. Under the plane-parallel homogeneous (PPH) assumption, the basic equation for the azimuth-averaged diffuse solar intensity $I(\tau, \mu)$ is given by equations (2.1)-(2.5) (the subscript wavenumber ν is omitted for simplicity of presentation),

$$\mu \frac{dI(\tau,\mu)}{d\tau} = I(\tau,\mu) - \frac{\omega}{2}\int_{-1}^{1} I(\tau,\mu')P(\mu,\mu')d\mu' - \frac{\omega}{4\pi}P(\mu,-\mu_0)F_0 e^{-\tau/\mu_0} \quad (3.1)$$

Where $\mu = cos\theta$, θ is the zenith angle, τ is the optical depth, ω is the single scattering albedo, $P(\mu,\mu')$is the azimuth-independent phase function, $F_0$is the direct solar irradiance (flux density) at top of atmosphere (TOA), and $\mu_0 = cos\theta_0$, θ_0 is the solar zenith angle. Three factors contribute to the source term: absorption, multiple scattering of diffuse intensity, and single scattering of direct solar irradiance (flux density) attenuated to the level τ.

The transfer of light beams in the atmosphere depends on the incoming and outgoing directions. It will be very complex and time consuming to solve equation (3.1) analytically. In order to obtain the upward and downward radiative fluxes, radiative transfer approximations are made. Some of the radiative transfer approximations, such as the two-stream approximation and Eddington's approximation, are widely used in the solar radiation calculation.

Replacing the integral with summation in equation (3.1), we have,

$$\mu_i \frac{dI(\tau,\mu_i)}{d\tau} = I(\tau,\mu_i) - \frac{\omega}{2}\sum_{j=-n}^{n} I(\tau,\mu_j)\, P_l(\mu_i,\mu_j)\, a_j - \frac{\omega}{4\pi}P(\mu_i,-\mu_0)F_0 e^{-\tau/\mu_0} \quad (3.2)$$

Where $i = -n, \ldots, n$. We may select the quadrature weights and points that satisfy $a_{-j} = a_j$ $(\sum_j a_j = 2)$ and $\mu_{-j} = -\mu_j$.

Rewrite equation (2.12) for the upward and downward fluxes as,

$$F^{\pm}(\tau) = 2\pi \int_0^1 I(\tau, \pm \mu)\mu d\mu \qquad (3.3)$$

Then the hemispheric integration of equation (3.1) can be expressed using the generalized two-stream approximation (Liou, 1992) by,

$$\frac{dF^{+}(\tau)}{d\tau} = \gamma_1 F^{+}(\tau) - \gamma_2 F^{-}(\tau) - \gamma_3 \omega F_0 e^{-\tau/\mu_0} \qquad (3.4a)$$

$$\frac{dF^{-}(\tau)}{d\tau} = \gamma_2 F^{+}(\tau) - \gamma_1 F^{-}(\tau) - (1 - \gamma_3)\omega F_0 e^{-\tau/\mu_0} \qquad (3.4b)$$

The coefficients γ_i $(i = 1, 2, 3)$ will be determined by the approximation method applied to the intensity and phase function.

For a plane-parallel homogeneous atmosphere with an optical depth τ, Meador and Weaver (1980) give a formal solution to equations (3.4a) and (3.4b). Define the reflectance *R* and total transmittance *T* as,

$$R(\tau, \mu_0) = \frac{F^{+}(0,\mu_0)}{\mu_0 F_0} \qquad (3.5a)$$

And

$$T(\tau, \mu_0) = \frac{F^{-}(\tau,\mu_0)}{\mu_0 F_0} + e^{-\tau/\mu_0} \qquad (3.5b)$$

Assuming the boundary conditions as, $F^{+}(\tau, \mu_0) = F^{-}(0, \mu_0) = 0$, the formal solution for equations (3.4a) and (3.4b) for the reflectance and transmittance are,

$$R(\tau, \mu_0) = \frac{\omega}{N}\left[(1 - k\mu_0)(\alpha_2 + k\gamma_3)\, e^{k\tau}\right.$$

$$\left. - (1 + k\mu_0)(\alpha_2 - k\gamma_3)\, e^{-k\tau} - 2k(\gamma_3 - \alpha_2\mu_0)\, e^{-\tau/\mu_0}\right] \qquad (3.6a)$$

$$T(\tau, \mu_0) = e^{-\tau/\mu_0}\left\{1 - \frac{\omega}{N}[(1 + k\mu_0)(\alpha_1 + k\gamma_4)\, e^{k\tau}\right.$$

$$- (1 - k\mu_0)(\alpha_1 - k\gamma_4)\, e^{-k\tau} - 2k(\gamma_4 + \alpha_1\mu_0)\, e^{-\tau/\mu_0}]\} \qquad (3.6b)$$

Where

$$N = (1 - k^2\mu_0^2)\left[(k + \gamma_1)\, e^{k\tau} + (k - \gamma_1)\, e^{-k\tau}\right]$$
$$\alpha_1 = \gamma_1\gamma_4 + \gamma_2\gamma_3$$
$$\alpha_2 = \gamma_1\gamma_3 + \gamma_2\gamma_4$$
$$k = (\gamma_1^2 - \gamma_2^2)^{1/2}$$
$$\gamma_4 = 1 - \gamma_3$$

In the two stream approximation, only the phase function is expanded in two terms in Legendre polynomials. In Eddington's approximation, both the intensity and phase function are expanded in two polynomial terms. Depending on the approximations to the intensity and phase function, various analytic forms for the coefficients γ_i can be derived. The coefficients for several selected two-stream approximations are given below (Liou 1992; King and Harshvardhan 1986),

Two-stream approximation:

$$r_1 = [1 - \omega(1 + g)/2]/\mu_1 \qquad (3.7a)$$
$$\gamma_2 = \omega(1 - g)/2\mu_1 \qquad (3.7b)$$
$$\gamma_3 = (1 - 3g\mu_1\mu_0)/2 \qquad (3.7c)$$

Where $\mu_1 = 1/\sqrt{3}$, and *g* is the asymmetry factor defined by,

$$g = \frac{\omega_1}{3} = \frac{1}{2}\int_{-1}^{1} P(cos\Theta)cos\Theta\, d\, cos\Theta$$

The asymmetry factor is the first moment of the phase function. Note the zero moment of the phase function equal to 1 ($\omega_0 = 1$). For isotropic scattering (such as Rayleigh scattering), the asymmetry factor is zero ($g = 0$).

Eddington's approximation:

$$\gamma_1 = [7 - \omega(4 + 3g)]/4 \quad (3.8a)$$

$$\gamma_2 = -[1 - \omega(4 - 3g)]/4 \quad (3.8b)$$

$$\gamma_3 = (2 - 3g\mu_0)/4 \quad (3.8c)$$

Practical Improved Flux Method (PIFM) (Zdunkowski et al. 1980):

$$\gamma_1 = [8 - \omega(5 + 3g)]/4 \quad (3.9a)$$

$$\gamma_2 = 3\omega(1 - g)]/4 \quad (3.9b)$$

$$\gamma_3 = (2 - 3g\mu_0)/4 \quad (3.9c)$$

Discrete-ordinates approximation (Liou 1973, 1974):

$$r_1 = \sqrt{3}\,[2 - \omega(1 + g)]/2 \quad (3.10a)$$

$$\gamma_2 = \sqrt{3}\,[\omega(1 - g)]/2 \quad (3.10b)$$

$$\gamma_3 = (1 - \sqrt{3}\,g\mu_0)/2 \quad (3.10c)$$

The GFS radiation scheme has included options for the last three approximations with the Delta-function adjustment (which is discussed in section 3.2).

3.2 Delta-function adjustment

In the discussions of the radiative transfer approximations in Section 3.1, the phase function is given by,

$$P(\mu, \mu') = 1 + 3g\mu\mu' \quad (3.11)$$

However, the phase functions involving cloud and aerosol particles are highly peaked in the forward direction, the two-term expansions do not adequately account for the strong forward scattering. Let *f* to be fraction of the energy scattered in the forward direction ($\Theta = 0$), the normalized phase function may be expressed as a Dirac delta function plus a two-term Legendre expansion,

$$P(\mu, \mu') = 2f\delta(\mu - \mu') + (1 - f)(1 + 3g^{*}\mu\mu') \quad (3.12)$$

Where $\mu = \mu'$ when $\Theta = 0$, δ is the Dirac delta function, $f = g^2$ is the forward scattering coefficient, and g^* is a scaled asymmetry factor.

After adding the delta function into the phase function, the original form of the radiative transfer equation (3.1) can still be held by taking the following transformations:

$$\tau \Rightarrow \tau^* = (1 - \omega f)\tau \quad (3.13a)$$

$$\omega \Rightarrow \omega^* = (1 - f)\omega/(1 - \omega f) \quad (3.13b)$$

$$g \Rightarrow g^* = (g - f)/(1 - f) \quad (3.13c)$$

Thus, the scaled optical depth, single scattering albedo, and asymmetry factor need to be used in the coefficients and solutions of the radiative transfer approximations when Delta-function adjustment is applied in the two-stream radiative transfer calculations.

3.3 Radiative flux calculations for solar radiation in PPH atmosphere

Radiative transfer theory has been elegantly developed under the assumption that the atmosphere is plane-parallel homogeneous (PPH). One of the approximation methods for the radiative transfer calculation is the generalized two-stream approximation, which has various analytic forms for the upward and downward intensity fields within and at the boundaries of a PPH medium. Three of these are included in GFS radiation calculation as options. The flux calculations discussed in this section apply to both band models and the correlated k-distribution method (discussed in section 6.1). Reflectance and transmittance of each atmospheric layer are first computed using two stream approximation with the Delta-function adjustment, fluxes are then computed by using a two-stream adding method for a composite of layers.

For each atmosphere layer and spectral interval, the effective optical thickness, single scattering albedo, asymmetry factor, and forward scattering coefficient are computed from,

$$\tau = \sum_i \tau_i \quad (3.14a)$$

$$\overline{\omega} = \sum_i \omega_i \tau_i / \sum_i \tau_i \quad (3.14b)$$

$$\overline{g} = \sum_i g_i \omega_i \tau_i / \sum_i \omega_i \tau_i \quad (3.14c)$$

$$\overline{f} = \sum_i f_i \omega_i \tau_i / \sum_i \omega_i \tau_i \quad (3.14d)$$

Where the summation is over all gasses and particles, *i* . They include water vapor, ozone, aerosols, clouds, and all atmospheric gasses.

Consider a two-layer case (layer 1 overlying layer 2), The reflectance and transmittance of a layer illuminated by a direct beam are calculated from equations (3.6a) and (3.6b) as a function of μ_0 and the optical properties τ, $\overline{\omega}$, and $\overline{g}$. For diffuse insolation, the reflectance r and transmittance t are also computed from equations (3.6a) and (3.6b) but the incident angles are approximated by a single value of 53^0,

$$r = R(\overline{\mu}) \tag{3.15a}$$

$$t = T(\overline{\mu}) \tag{3.15b}$$

Where $\overline{\mu} = cos(53^0)$.

By separating the direct and diffuse components of the radiation, the reflectance and the total transmittance of the layer when illuminated by direct radiation can be computed using a two stream adding method (Hou et al. 2002, Chou 1992, Oreopoulos and Barker 1999) as,

$$R_{1,2}(\mu_0) = R_1(\mu_0) + t_1[(T_1(\mu_0) - T_1^{dir}(\mu_0))\, r_2 + T_1^{dir}(\mu_0)\, R_2(\mu_0)]/(1 - r_1 r_2) \tag{3.16a}$$

$$T_{1,2}(\mu_0) = T_1^{dir}(\mu_0) T_2(\mu_0) + t_2[(T_1(\mu_0) - T_1^{dir}(\mu_0)) + T_1^{dir}(\mu_0)\, R_2(\mu_0)\, r_1]/(1 - r_1 r_2) \tag{3.16b}$$

And

$$T_{1,2}^{dir}(\mu_0) = T_1^{dir}(\mu_0)\, T_2^{dir}(\mu_0) \tag{3.17}$$

Where

$$T_1^{dir}(\mu_0) = e^{-\tau_1/\mu_0} \tag{3.18}$$

is the direct solar beam transmission for layer 1, τ_1 is the mean optical depth of the upper layer, and $T(\mu_0)$, $e^{-\tau/\mu}$, and $(T(\mu_0) - e^{-\tau/\mu})$ are total, direct, and diffuse transmissivities, respectively.

If the source is diffuse irradiance, the combined reflectance to diffuse radiation can be expressed in two situations: one is the upper layer illuminated by diffuse radiation, and the other is that lower layer illuminated,

$$r_+ = r_{1,2} = r_1 + t_1^2 r_2 / (1 - r_1 r_2) \quad (3.19a)$$

$$r_- = r_{2,1} = r_2 + t_2^2 r_1 / (1 - r_1 r_2) \quad (3.19b)$$

When illuminated by a direct beam radiation at the top of the layer, the reflectance $R^{\uparrow}$, and the transmittance, $T^{\downarrow}$, at the interface of the sublayers 1 and 2 are given by,

$$R^{\uparrow} = \left[e^{-\tau_1/\mu_0} R_2(\mu_0) + (T_1(\mu_0) - e^{-\tau_1/\mu_0}) r_2 \right] / (1 - r_1 r_2) \quad (3.20a)$$

$$T^{\downarrow} = e^{-\tau_1/\mu_0} + [e^{-\tau_1/\mu_0} r_1 R_2(\mu_0) + (T_1(\mu_0) - e^{-\tau_1/\mu_0})] / (1 - r_1 r_2) \quad (3.20b)$$

For a multi-layered atmosphere, by using a two-stream adding method (Chou and Suarez 1999), one can obtain normalized fluxes at layer interfaces through two calculation passes. The first starts from the top and adds one layer at a time until it reaches the bottom surface. During this pass, the total downward transmission at each level, $T(\mu_0)$, and the diffuse reflectance for layers illuminated from below, r_-, are computed. The second pass starts from the bottom surface and works one layer at a time to the top to obtain the reflectance to the direct radiation, $R(\mu_0)$, at each level, and the diffuse reflectance, r_+, for layers illuminated from above. Thus the normalized upward and downward fluxes at the lower boundary of layer k are given as (Hou et al. 2002),

$$F^{\uparrow}_{k+1/2}(\mu_0) = [T^{\downarrow}_k(\mu_0) R_{k+1}(\mu_0)$$

$$+ \ (T_k(\mu_0) - T_k^{\downarrow}(\mu_0))\, r_{+,k+1}]/(1 - r_{-,k}\, r_{+,k+1}) \qquad (3.21a)$$

$$F_{k+1/2}^{\downarrow}(\mu_0) = T_k^{\downarrow}(\mu_0) + [T_k^{\downarrow}(\mu_0) R_{k+1}(\mu_0)\, r_{-,k}$$

$$+ \ (T_k(\mu_0) - T_k^{\downarrow}(\mu_0))]/(1 - r_{-,k}\, r_{+,k+1}) \qquad (3.21b)$$

At the top of the atmosphere (*k=1*), then,

$$F_{1-1/2}^{\uparrow}(\mu_0) = R_1(\mu_0) \quad \text{and} \quad F_{1-1/2}^{\downarrow}(\mu_0) = 1 \qquad (3.22)$$

The total net flux at each pressure level (at a layer interface) and at the surface is the weighted sum of these fluxes,

$$F_{net}(\mu_0, p) = F_0 \mu_0 \sum_i \psi_i \, [\, F_i^{\downarrow}(\mu_0, p) - F_i^{\uparrow}(\mu_0, p) \,] \qquad (3.23)$$

Where F_0 is the incoming solar flux at the top of the atmosphere, *i* is the index of spectral band, and ψ_i is the weight for the corresponding band, and the sum of ψ_i is 1.

4. Thermal Infrared Radiative Transfer

Thermal infrared radiation plays an important role in the global energy budget and maintaining the climate system. The equilibrium temperature of the earth-atmosphere system is about 255 K. The spectrum of the thermal infrared radiation from Earth and its atmosphere to space spans from 3 μm to 100 μm. Just as the major atmospheric gasses (oxygen and nitrogen) are transparent to incoming sunlight, they are also transparent to outgoing thermal infrared. However, water vapor, carbon dioxide, methane, and other trace gasses are opaque to many wavelengths of thermal infrared energy. A significant amount of the infrared radiative energy emitted by the earth's surface (~116 units) is absorbed by the atmospheric greenhouse gasses (~104 units) and radiative back to the earth's surface (~98 units) (assuming the incoming solar radiation at TOA is 100 units). Cloud is also strongly coupled with longwave radiation. Thick optical clouds absorb longwave irradiance emitted by the Earth's surface near the cloud base and emit at a colder temperature near the cloud top,

therefore longwave radiation cools the cloud top and warms the cloud base and impacts the cloud dynamics.

4.1 Longwave Radiative Transfer Approximation

In a plane-parallel homogeneous atmosphere, the azimuth-averaged diffuse long wave intensity $I(\tau, \mu)$ is governed by the equation (again, the subscript of wavenumber ν is omitted for simplicity of presentation),

$$\mu \frac{dI(\tau,\mu)}{d\tau} = I(\tau,\mu) - \frac{\omega}{2}\int_{-1}^{1} I(\tau,\mu')P(\mu,\mu')d\mu' - (1-\omega)B(\theta) \qquad (4.1)$$

Where $\mu = cos\theta$, θ is the zenith angle, τ is the optical depth, ω is the single scattering albedo, $B(\theta)$ is the Planck Function for substance with temperature θ, and $P(\mu, \mu')$ is the azimuth-independent phase function. The phase function can be expanded in Legendre polynomials as Equation (2.10).

Replacing the integral with summation in equation (4.1), and selecting the Gauss quadrature weights and points, the discrete-ordinates approximation can be expressed as (Liou, 2002),

$$\mu_i \frac{dI(\tau,\mu_i)}{d\tau} = I(\tau,\mu_i) - \frac{\omega}{2}\sum_{j=-n}^{n} I(\tau,\mu_j)\, P_l(\mu_i,\mu_j)\, a_j - (1-\omega)B(\theta) \qquad (4.2)$$

Where $i = \pm 1, \ldots, \pm n$, quadrature point $\mu_{-j} = -\mu_j$, $j \neq 0$, weight $a_{-j} = a_j$. The longwave scattering effect has been neglected in most current climate models. Zhao et al. (2018) studied the cloud longwave scattering effect using the eight-stream DISORT scheme in RRTMG_LW and CAM5. Results show that the cloud longwave scattering reduces the flux at the TOA and leads to an extra warming effect in the atmosphere. The warming mainly concentrates in the low level rising branch of the Hadley circulation, and modulates the westerly jet and upper part of the Walker circulation.

The phase function $P(\mu, \mu')$ can be expanded using δ-Eddington approximation as,

$$P(\mu,\mu') = 2f\,\delta(\mu-\mu') + (1-f)(1+3g\mu\mu' + \ldots) \qquad (4.3)$$

where *f* is the fractional scattering into the forward direction, *g* is the asymmetry factor. When LW absorption is strong enough to overwhelm scattering, the process can be simplified by

setting f = 1, which means only the forward-scattering peak is kept and scattering in all the other directions is completely neglected. Then Equation (4.1) can be written as,

$$\mu \frac{dI(\tau,\mu)}{d\tau} = (1 - \omega)\, I(\tau,\mu) - (1 - \omega)\, B(\theta) \qquad (4.4)$$

where μ is cosine of the local zenith angle, τ is the optical depth, ω is the single scattering albedo, and $B(\theta)$ is blackbody emission at temperature θ. Equation (4.4) is referred to as an absorption approximation (AA), which is more accurate than the method that completely ignores the scattering effect. Since absorption approximation only keeps the forward scattering, upward flux and downward flux can be calculated independently. The upward flux at pressure *p* is given as (Li, 2000),

$$F^{\uparrow} = B(\theta_s)\, T[\tau_v(p,p_s)] - \pi \int_{p}^{p_s} B(\theta') \frac{\partial T[\tau(p,p')]}{\partial p'} dp' \qquad (4.5)$$

The downward flux at pressure *p* is,

$$F^{\downarrow} = \pi \int_{0}^{p} B(\theta') \frac{\partial T[\tau(p,p')]}{\partial p'} dp' \qquad (4.6)$$

where p_s is the surface pressure, θ_s is the surface temperature, θ' is the temperature at pressure *p′*, and $T[\tau(p,p')]$ is the flux transmittance defined in terms of the optical depth $\tau(p,p')$ for a slab of atmosphere between *p* and *p′*,

$$T[\tau(p,p')] = 2 \int_{0}^{1} exp\left[-\tau_{abs}(p,p')/\mu\right] \mu d\mu \qquad (4.7)$$

Where

$$\tau_{abs}(p,p') = \int_{p'}^{p} [1 - \omega(p'')] \frac{\partial \tau(p,p'')}{\partial p''}\, dp'' \qquad (4.8)$$

In a clear-sky, $\omega = 0$, the integration (4.7) can be approximated as (Elsasser 1942),

$$T[\tau] = 2 \int_{0}^{1} exp\left[-\tau_{abs}/\mu\right] \mu d\mu \approx exp(-\tau_{abs}/\mu_1) \qquad (4.9)$$

Where μ_1 = 1/1.6487 is the diffusivity factor. Accurate integration of directional radiance shows that the conventional diffusivity-factor approximation with a constant diffusivity angle results in an overestimation of the outgoing longwave radiation (OLR) in the window band and an underestimation in the absorption band. For more accurate longwave flux calculations, the RRTMG_LW performs radiative transfer for a single (diffusivity) angle (angle = 53 deg; secant angle = 1.66) and improves accuracy in profiles with high water content by varying the angle in some bands as a function of total column water.

The advantage of Eq. (4.9) is that the flux transmittance follows a simple exponential decay law, in the same manner as the radiance transmittance. The definition of the flux transmittance in terms of an exponential function is efficient for a multilayer calculation. If the flux transmittance for each layer is known, the result for any combined adjacent layers is the multiple of the results for each layer, since for two layers of optical depths τ_i and τ_j,

$$T(\tau_i + \tau_j) = T(\tau_i)\, T(\tau_j) \tag{4.10}$$

In the infrared, each layer of the model contains a heat source. One, therefore, needs to be able to calculate the transmittance between layers that are at varying separation. The simple multiplicative nature of the approximation shown in Eq.(4.10) avoids additional computation of exponentials.

4.2 Radiative flux calculation for longwave radiation in PPH atmosphere

Radiative flux calculation for longwave radiation is relatively simple. The discrete form of equations (4.5) and (4.6) can be written as,

$$F_i^{\uparrow} = \pi \sum_{k=i}^{N-1} B_{k+(1/2)} \left(T_{i,k+1} - T_{i,k}\right) + B_s T_{i,N} \tag{4.11a}$$

$$F_i^{\downarrow} = \pi \sum_{l=1}^{i-1} B_{l+(1/2)} \left(T_{l,i} - T_{l+1,i}\right) \tag{4.11b}$$

Where $F_i^{\uparrow}$ ($F_i^{\downarrow}$) is the upward (downward) flux at level *i*, $T_{k,l}$ is the transmittance between two levels *k* and *l*, $B_{i+1/2}$ is the Planck function for layer *i* (between level *i* and level *i* + *1*), level 1 is the top of the atmosphere, and level *N* is the surface.

If we focus on one single layer with optical depth $\Delta\tau$, the downward (upward) flux at the bottom (top) of the layer is,

$$F_{out} = F_{in} e^{-\Delta\tau/\mu_1} + B^* (1 - e^{-\Delta\tau/\mu_1}) \quad (4.12)$$

Where F_{out} is the outgoing flux, F_{in} is the incoming flux, B^* is the effective Planck function which is discussed below, μ_1 is the diffusivity factor.

Following Clough et al (1992), assuming the Planck function varies linearly with optical depth from the value at the upper boundary B_U to that at the lower boundary B_L with slope $(B_U - B_L)/\tau$, the radiance source term in the layer can be computed as,

$$I = B_U(1 - T) - (B_L - B_U)T + \left(\frac{B_L - B_U}{\tau}\right)(1 - T) \quad (4.13)$$

Where τ and T are the optical depth and associated transmittance of the layer. Equation (4.13) is commonly referred to as "linear in Tau" approximation. In the limit of strong absorption, the radiance goes to B_U, in the limit of weak absorption, $I = \tau \overline{B}$, where $\overline{B}$ is the mean Planck function for the layer, and $\overline{B} = (B_U + B_L)/2$.

Writing equation (4.13) in terms of mean Planck function, we have,

$$I = (1 - T)\left[B_U + 2 (\overline{B} - B_U) (\frac{1}{\tau} - \frac{T}{1-T}) \right] \quad (4.14a)$$

Define the effective Planck function $B^*(\tau)$ as,

$$B^*(\tau) = B_U + 2 (\overline{B} - B_U) (\frac{1}{\tau} - \frac{T}{1-T}) \quad (4.15)$$

equation (4.14a) can be written as,

$$I = (1 - T) B^*(\tau) \quad (4.14b)$$

In the line-by-line radiance calculation (LBLRTM), the empirical formulation of the effective Planck function in equation (4.15) is computed as a one-term Pade approximation as,

$$B^*(\tau) = [\overline{B} + (a\,\tau) B_U]/ (1 + a\,\tau) \quad (4.16a)$$

Where $a = 0.278$ is used in RRTMG code. There is also a two-term Pade approximation in literature as,

$$B^{*}(\tau) = [\overline{B} + (a\,\tau + b\,\tau^{2})\,B_{U}]/(1 + a\,\tau + b\,\tau^{2}) \qquad (4.16b)$$

With *a=0.193, b=0.013*. The one-term Pade approach $a = 0.2$ has been implemented in the FASCODE (Clough et al 1992).

Solutions (4.11) and (4.12) are equivalent. In solution (4.11) the upward (downward) flux at one level is determined by the thermal emission and absorption from all the layers below (above) that level. Therefore, the computing time is quadratically proportional to the number of model layers. In Eq. (4.12) all the exchange contributions from outside of this layer are represented by the boundary conditions. Therefore, the computing time is linearly proportional to the number of the model layers.

Considering a PPH atmospheric layer, the radiative flux at wavenumber υ can be calculated using equation (4.12), and the spectrally averaged outgoing radiance from the atmospheric layer is (this equation is used in RRTMG LW),

$$\overline{R}'_{\upsilon_1,\upsilon_2} = \frac{1}{\upsilon_2-\upsilon_1}\int_{\upsilon_1}^{\upsilon_2} d\upsilon\,[B^{*}(\upsilon,T_{\upsilon}) + [R_0(\upsilon) - B^{*}(\upsilon,T_{\upsilon})]\,exp\left(-\,k(\upsilon,P,\theta)\,\frac{\rho\Delta z}{\mu_1}\right) \qquad (4.17)$$

Where υ_1 and υ_2 are the beginning and ending wavenumbers of the spectral interval, R_0 is the incoming radiance to the layer, $B^{*}(\upsilon,T_{\upsilon})$ is an effective Planck function for the layer, T_{υ} is the transmittance for the layer optical path, $k(\upsilon,P,\theta)$ is the absorption coefficient at layer pressure *P* and temperature θ, and ρ is the absorber density.

In band model, the total net flux at each pressure level (at a layer interface) and at the surface is the weighted sum of fluxes from each spectral interval,

$$F_{net}(\mu_0,\,p) = \sum_n \psi_n\,[\,F_n^{\downarrow}(\mu_0,\,p) - F_n^{\uparrow}(\mu_0,\,p)\,] \qquad (4.18)$$

Where *n* is the index of spectral interval, and ψ_n is the weight for the corresponding spectral interval, and the sum of ψ_n is 1, and $F_i^{\uparrow}$ ($F_i^{\downarrow}$) is the average upward (downward) flux over the spectral interval from equation (4.17).

The above calculation is extended to obtain the radiative transfer for vertically inhomogeneous atmospheres by dividing the atmosphere into layers. Using the outgoing radiance at each interval as the incoming radiance for the same interval of the adjacent layer, the average outgoing radiative flux can be obtained using equation (4.17), and the total flux is the sum of all the spectral intervals from equation (4.18). In the k-distribution method, each band (or spectral interval) includes a different number of subintervals, we need to sum over all the subintervals and over all the bands in equation (4.18).

5. Radiative Flux Calculations for Partially Cloudy Sky

Clouds could occur at various heights with different fractional cover and optical properties. Nearly all radiative transfer algorithms used in atmospheric models apply only to a plane-parallel homogeneous (PPH) atmosphere. Horizontal inhomogeneity is not allowed. An approach to dealing with partial cloudiness is to divide a region into subcolumns and assume that radiation flows through each subcolumn independently of all other subcolumns, regardless of the cross-sectional areas of the subcolumns, and that flow through each subcolumn can be described by 1D radiative transfer theory. This is the independent column (or pixel) approximation (ICA or IPA). Within each subcolumn, an atmospheric layer (each subcolumn can be divided into many layers) is either free of clouds or filled totally with a homogeneous cloud. Domain-averaged fluxes in variable clouds can be determined quite accurately using ICA approximation by averaging the flux computed for each class of clouds in turn (Cahalan et al. 1994; Barker et al. 1999). Depending on the number of cloud layers and the way these clouds overlap, computation can be very expensive. Radiative transfer calculation is time consuming because fluxes and heating rates are broadband quantities that must be integrated over many spectral intervals. A heating rate profile in a single column is, in fact, the result of many narrowband calculations.

Monte Carlo Independent Column Approximation (McICA) (Pincus et al. 2003) is a computationally efficient technique for computing domain-averaged broadband radiative fluxes in vertically and horizontally variable cloud fields of arbitrary complexity. The method makes random, uncorrelated errors in estimates of radiative quantities, and the expectation value of these estimates is completely unbiased with respect to the ICA.

5.1 Monte Carlo Independent Column Approximation (McICA)

McICA is an approximation to the full independent column approximation (ICA) when computing grid-box mean fluxes. In the full ICA, domain-average broadband radiative fluxes are computed as (Pincus et al. 2003; Raisanen and Barker 2004),

$$\overline{F} = \frac{1}{N} \sum_{n=1}^{N} F_n \tag{5.1}$$

Where *N* is the number of subcolumns and F_n is the broadband radiative flux for the n^{th} subcolumn. The broadband radiative fluxes for the n^{th} subcolumn are computed as the summation over all spectral intervals of the broadband,

$$F_n = \sum_{k=1}^{K} c_k F_{n,k} \tag{5.2}$$

Where *K* is the total number of spectral intervals, c_k is weight in each spectral interval, and $F_{n,k}$ indicates fluxes computed using one-dimensional radiative transfer theory from k^{th} spectral interval.

Combining equations (5.1) and (5.2), we have the domain-averaged broadband fluxes for the full ICA as,

$$\overline{F} = \overline{F}^{ICA} = \frac{1}{N} \sum_{n=1}^{N} \sum_{k=1}^{K} c_k F_{n,k} \tag{5.3}$$

Radiative fluxes are more uniform in clear skies than in clouds, so the domain is partitioned into clear and cloudy portions and a single calculation is performed for the clear sky. Because each subcolumn is treated independently, we may write equations (5.3) as an summation over the distribution *p(s)* of possible states *s* of the cloudy atmosphere (with potentially unequal weights *w*),

$$\overline{F}^{ICA} = (1 - C_{tot}) \sum_{k}^{K} w_k c_k F_k^{clr} + C_{tot} \sum_{k}^{K} w_k c_k \sum_{n=1}^{N_{cld}} p(s_n) F_{n,k}^{cld}$$

$$= (1 - C_{tot})\,\overline{F}^{clr} + C_{tot}\,\overline{F}^{cld} \qquad (5.4)$$

Where C_{tot} is the total cloud fraction for the GCM column, and N_{cld} is the total number of cloud states of the cloudy atmosphere, and $N_{cld} \leq N$. Equation (5.4) is general and applies to any method of solving the radiative equation. The spectral intervals may be thought of as bands (e.g., Slingo, 1989) or as the quasi-monochromatic intervals in a k-distribution. It is the nested sum in the last term in equation (5.4) that makes the ICA impractical in large scale models.

The full ICA calculation of cloudy-sky flux $\overline{F}^{cld}$ is a two-dimensional summation, with wavelength varying in one-dimension and cloud state in the other. Rather than computing the contribution of every cloud state to every wave interval, the $\overline{F}^{cld}$ is approximated by choosing a cloud state at random for each spectral interval,

$$\overline{F}^{cld} \approx \sum_{k}^{K} w_k\, c_k\, F_{n_{k'}k} \qquad (5.5)$$

Where $F_{n_{k'}k}$ is the monochromatic radiative flux in spectral interval *k*, with a randomly selected vertical cloud distribution n_k. Equation (5.5) is a Monte Carlon summation of the ICA, or referred to as the McICA. From this definition, the McICA solution (5.5) is equal to the ICA solution only when all *N* subcolumns are identical or when *N=1*. As discussed in Pincus et al (2003), McICA's incomplete pairing of subcolumns and spectral intervals ensures that its solution will contain random, but unbiased, errors. Direct application of equation (5.5) requires *K* cloudy-sky calculations per domain.

5.2 Cloud overlapping method

The current operational GFS uses the exponential-random (EXP-RAN) cloud overlapping scheme. Cloud overlap is usually defined in terms of three basic idealized assumptions: maximum, minimum, or random. Considering cloud cover in two layers and assuming the cloud fraction is given by C_k and C_l, then the three assumptions can be described by the combined total cloud cover as,

Maximum overlap: $C_{k,l}^{max} = max\,(C_k,\, C_l)$ (5.6a)

Minimum overlap: $C_{k,l}^{min} = min\,(C_k + C_l, 1)$ (5.6b)

Randomly overlap: $C_{k,l}^{ran} = C_k + C_l - C_k C_l$ (5.6c)

The maximum-random (MAX-RAN) overlap scheme assumes that clouds in adjacent vertical levels are likely to form from part of the same vertical cloud element and are maximally overlapped, while clouds separated by a clear layer are assumed to be spatially decorrelated and thus randomly overlapped (e.g., Geleyn and Hollingsworth 1979).

In nature, the observed total cloud cover resulting from the overlap of two layers in any particular cloud scene $C_{k,l}$ is unlikely to equal that given by one of the above assumptions. Barker et al. (1999) used cloud resolving model output to show that the overlap of continuous clouds often lies between MAX and RAN for the scenes studied. It is useful to express the observed total cloud cover as a linear combination of MAX and RAN using the overlap parameter $\alpha_{k,l}$ (Hogan and Illingworth, 2000),

$$C_{k,l} = \alpha_{k,l} C_{k,l}^{max} + (1 - \alpha_{k,l}) C_{k,l}^{ran} \quad (5.7)$$

It is apparent that $\alpha_{k,l} = 1$ gives maximally overlapped layers, and $\alpha_{k,l} = 0$ gives random overlap. Note that observed total cloud cover of the two layers can exceed the random overlap value, as in the case of minimum overlap, for which $\alpha_{k,l}$ will assume a negative value. Observations indicate that $\alpha_{k,l} < 0$ occurs much less frequently for adjacent layers than for distant ones, so it is assumed $\alpha_{k,l} \geq 0$ and the overlap can be described adequately by applying (5.7) successively to adjacent layers and thus working directly with $\alpha_{k-1,k}$ only. For non-adjacent layers the overlap parameter is defined implicitly as,

$$\alpha_{k,l} = \prod_{m=k+1}^{l} \alpha_{m-1,m} \quad (5.8)$$

For each of the layer pairs, $\alpha_{k,l}$ has been calculated as a function of the inter-layer separation distance. The reduction of $\alpha_{k,l}$ is modeled by assuming an exponential decay of the separation distance Δz,

$$\alpha_{k,l} = exp\left(-\frac{\Delta z}{L\,(z)}\right) \quad (5.9)$$

Where L is a decorrelation length for overlapping fractional clouds. The decorrelation length scale is in the range of 2-4 km (can be a constant or latitude dependent parameter). Using $\alpha_{k,l}$ from equation (5.9), then equation (5.7) becomes an exponential-random cloud overlapping scheme (EXP-RAN).

There are several different formulations for the decorrelation length in the EXP-RAN scheme. The decorrelation length in GFS operational model uses Hogan's formulation (2010) with slightly different coefficients,

$$L(z) = 2.78 - 0.025556\,\phi$$

Where ϕ is the absolute latitude in degrees.

There are various versions of maximum-random cloud overlap generators. Here we discuss the version from Geleyn and Hollingsworth (1979) (Raisanen et al. 2004). Considering a partially cloudy atmosphere, let *N* be the total number of spectral intervals, we divide the atmospheric column into *N* subcolumns. We assume that the atmosphere is discretized into *K* layers, the uppermost being *k=1*. In order to apply the 1D radiative transfer theory, it is further assumed that each layer of each subcolumn is either filled with or free of clouds (horizontally homogeneous). Therefore, cloud fraction $c_{j,k}$ in the k^{th} layer of the j^{th} subcolumn is either 0 or 1. The cloud generator is an algorithm that determines $x_{j,k}$ $(0 \le x_{j,k} \le 1)$ for each subcolumns *j* and layer *k*. Properties of the generated fields depend on how $x_{j,k}$ is determined as well as on conditions provided by the global model. The variable $x_{j,k}$ is used to decide whether the cells of subcolumns are cloudy or clear according to,

$$c_{j,k} = 0, \quad if\ x_{j,k} \le 1 - C_k \ \text{(clear)}$$
$$c_{j,k} = 1, \quad if\ x_{j,k} > 1 - C_k \ \text{(cloudy)}$$

Where $k = k_{top}, \ldots, k_{base}$ (k_{top} and k_{base} are the uppermost and lowermost layers with $C_k > 0$), and C_k is the cloud fraction for the k^{th} layer. The cloud fraction is either computed from a RH (relative humidity) based empirical scheme or a PDF based statistical scheme (Tompkins, 2005). For the GFDL microphysics scheme, the cloud fraction is calculated in the microphysics subroutine assuming a uniform distribution of total water. For other microphysics schemes, if cloud fraction is not calculated in the microphysics subroutine, the

cloud fraction is computed in the cloud scheme subroutine using the parameterization scheme of Xu and Randall (1996).

$$C_k = RH^{k_1}\left\{1 - exp(-k_2 q_l / \left[(1 - RH)\, q_s\right]^{k_3}\right\} \quad if\ RH < 1 \qquad (5.10a)$$

$$C_k = 1 \quad if\ RH \geq 1 \qquad (5.10b)$$

Where *RH* is relative humidity, q_l is the cloud condensate, q_s is saturation specific humidity, $k_1 = 0.25$, $k_2 = 100$, $k_3 = 0.49$ are the empirical parameters.

Beginning at k_{top}, this algorithm determines $x_{j,k}$, by first assigning to each subcolumn

$$x_{j,k_{top}} = RN1_{j,k_{top}}, \quad j = 1, \ldots, N$$

Where $RN1_{j,k_{top}}$ is a unique random number distributed evenly between 0 and 1. For subsequent layers,

$$x_{j,k} = x_{j,k-1} \quad if\ x_{j,k-1} > 1 - C_{k-1} \quad \text{(cloudy cell above)}$$

$$x_{j,k} = RN_{j,k}(1 - C_{k-1}) \quad if\ x_{j,k-1} \leq 1 - C_{k-1} \quad \text{(cloudless cell above)}$$

Where $k = k_{top+1}, \ldots, k_{base}$, and $RN_{j,k}$ are new random numbers with properties like $RN1_{j,k_{top}}$. Because horizontally homogeneous clouds are assumed, mean cloud water content for the cloudy part of a model layer is assigned to each cloudy cell in that layer.

In the Geleyn and Hollingsworth's (1979) version of the maximum-random overlap (MRO), total cloud fraction for layers k through l, inclusive, is

$$C_{k\to l} = 1 - (1 - C_k) \prod_{m=k+1}^{l} \frac{1 - max(C_{m-1}, C_m)}{1 - C_{m-1}} \qquad (5.11)$$

After computing the net radiation fluxes separately for clear-sky ($F_{net-clr}$) and for cloudy-sky ($F_{net-cld}$), the net flux for total sky is computed as a simple linear combination of

clear-sky and cloudy-sky quantities weighted by their respective fractions (Morcrette and Fouquart 1986),

$$F_{net-tot}(k) = (1 - C_{tot})\, F_{net-clr}(k) + C_{tot}\, F_{net-cld}(k) \qquad (5.12)$$

The temperature change for layer k due to solar and thermal infrared radiation is then calculated from,

$$\frac{dT_k}{dt} = -\frac{g}{C_p}\frac{dF_{net}(k)}{dp} \qquad (5.13)$$

Where T_k is the temperature at layer *k*, *t* is time, g is the gravitational acceleration, and C_p is the heat capacity of air at constant pressure.

5.3 Cloud optical properties

The cloud optical properties needed for the radiative transfer calculations in weather models are the volume extinction coefficient, the single scattering albedo, and the asymmetry factor. Depending on the cloud microphysics scheme used in the model, cloud optical properties are calculated differently. The GFS cloud-optics module uses the in-cloud liquid water and ice mixing ratios to calculate 1) the layer total cloud fraction, 2) layer cloud liquid water path, ice water path, rainwater path and snow water path, 3) mean effective radius for liquid cloud, ice cloud, raindrop and snowflake. Finally, the cloud optical properties for shortwave and long wave are parameterized using LWP (IWP) or LWC (IWC) and the effective radius of water droplets or ice particles.

5.3.1 Liquid water cloud

The parameterizations of optical properties for liquid water clouds follows Hu and Stamnes (1993). Assuming water cloud droplets are spherical particles, and have droplet size distribution, *n(r)*, the liquid water content (LWC, $g\ cm^{-3}$) is given by,

$$LWC = \frac{4\pi}{3}\,\rho_l \int r^3 n(r)\, dr \qquad (5.14)$$

And the liquid water path (LWP) is,

$$LWP = \Delta z \cdot (LWC) \qquad (5.15)$$

Where Δz is the cloud layer thickness, r is the radius of droplets, and ρ_l is the density of liquid water.

The effective radius for liquid water cloud is defined as,

$$r_{ew} = \int n(r)\, r^3 dr \,/\, \int n(r)\, r^2 dr \tag{5.16}$$

The extinction and scattering coefficients are,

$$\beta_{ext} = \frac{\pi}{k^3} \int_0^\infty n(r)\, r^2\, Q_{ext}(r)\, dr \tag{5.17}$$

$$\beta_{sca} = \frac{\pi}{k^3} \int_0^\infty n(r)\, r^2\, Q_{sca}(r)\, dr \tag{5.18}$$

Where $k = 2\pi\lambda^{-1}$, λ is the wavelength, Q_{ext} and Q_{sca} are the extinction efficiency and scattering efficiency, respectively. We may compute Q_{ext} and Q_{sca} by Mie theory for a number of radii r spanning the droplet sizes of interest and then perform the necessary integrations over the size distribution to determine β_{ext} and β_{sca} from equations (5.17) and (5.18). The single-scattering albedo ω and asymmetry factor are,

$$\omega = \beta_{sca} / \beta_{ext} \tag{5.19}$$

$$g = \frac{1}{2} \int_{-1}^{1} P(\mu)\, \mu\, d\mu \tag{5.20}$$

Where μ is the cosine of the scattering angle and $P(\mu)$ is the phase function.

Hu and Stamnes (1993) generated a group of data relating the optical properties to cloud liquid water content and equivalent radius for a variety of cloud size distributions with equivalent radii ranging from 2.5 to 60 μm. The data are used to parameterize the extinction coefficient β_{ext} , the scattering albedo ω, and the asymmetry factor g for both the solar and terrestrial wavelengths:

$$\beta_{ext} / LWC = a_1 r_{ew}^{b_1} + c_1 \tag{5.21a}$$

$$1 - \omega = a_2 r_{ew}^{b_2} + c_2 \quad (5.21b)$$

$$g = a_3 r_{ew}^{b_3} + c_3 \quad (5.21c)$$

Where LWC is the liquid water content of the cloud and $(1 - \omega)$ is the coalbedo. In the parameterization, the equivalent radius is in units of micrometers. All of the coefficients a_i, b_i, c_i (i=1,2,3) in equations (5.21a) to (5.21c) are constants for a given wavelength.

Using the least-squares method, the data are fitted in the following three radii ranges: 1) small size 2.5 to 12 μm, 2) medium range 12 to 30 μm, 3) large size 30 to 60 μm. The data are separated into 24 bands in the visible and near infrared part of the spectrum (0.3 - 4.0 μm) and 50 bands in the infrared (terrestrial) spectrum (4.0-150.0 μm). The coefficients a_i, b_i, c_i (i=1,2,3) for the fitting in the shortwave and longwave regions are given by Hu and Stamnes (1993).

Depending on the microphysics schemes used, several options are available to calculate the LWP and the effective radius of the liquid water cloud in the GFS cloud schemes. Some options are discussed below,

For GFDL microphysics (Lin et al. 1983; Chen and Lin 2011, 2013), the total cloud condensate path is calculated (large scale cloud condensate path + convective cloud condensate path), and then partitioned into LWP and IWP based on environmental temperature. The fraction of the ice cloud is parameterized as a function of temperature,

$$F = min[1, max(0, (273.16K - T)/20))] \quad (5.22a)$$

and the LWP and IWP are separated as,

LWP = total cloud condensate path * $(1 - F)$ (5.22b)

IWP = total cloud condensate path * F (5.22c)

The effective radius is parameterized as follows,

$r_{ew} = 10\ \mu m$ over ocean (5.23a)

$r_{ew} = 5.0 + 5.0 \cdot F$ over land (5.23b)

For Thompson microphysics scheme (Thompson and Eidhammer 2014) and WSM6 microphysics scheme (Hong and Lim 2006), the cloud liquid water path is calculated using

equation (5.15), and the effective radius is given from the microphysics schemes. The rainwater path is calculated similar to equation (5.15), and the effective radius for rainwater is set to be constant at 1000 μm.

5.3.2 ice cloud

The parameterizations of the solar radiative properties and infrared radiative properties for ice clouds follow Fu (1996), and Fu et al. (1998), respectively. Assuming n*(L)* denotes the ice crystal size distribution, L_{min} and L_{max} are the minimum and maximum lengths of ice crystals, respectively, and ρ_i is the density of ice, we have the ice water path,

$$IWP = \Delta z \int V \rho_i \, n(L) \, dL = \Delta z \cdot (IWC) \tag{5.24}$$

Where Δz is the cloud layer thickness, V is the volume of an individual ice crystal, L is the major dimension, and IWC is the ice water content.

For a given ice crystal size distribution, the single scattering properties of ice clouds, including the extinction coefficient (β), absorption coefficients (β_a), and the asymmetry factor (g) may be obtained from,

$$\beta = \int_{L_{min}}^{L_{max}} Q(L) \, P(L) \, n(L) \, dL \tag{5.25a}$$

$$\beta_a = \int_{L_{min}}^{L_{max}} Q_a(L) \, P(L) \, n(L) \, dL \tag{5.25b}$$

$$g = \int_{L_{min}}^{L_{max}} Q_s(L) \, P(L) \, g_L \, n(L) \, dL \Big/ \int_{L_{min}}^{L_{max}} Q_s(L) \, P(L) \, n(L) \, dL \tag{5.25c}$$

Where Q, Q_a and Q_s are the extinction, absorption, and scattering efficiencies, respectively, for a random oriented hexagonal ice crystal, g_L is the asymmetry factor, and P is the projected area.

By assuming that ice crystals are hexagonal, the ice water content (IWC) and generalized effective size (D_{ge}) are defined in the forms,

$$IWC = \frac{3\sqrt{3}}{8} \rho_i \int_{L_{min}}^{L_{max}} D^2 L\, n(L) dL \quad (5.26)$$

And

$$D_{ge} = \int_{L_{min}}^{K_{max}} D^2 L\, n(L) dL \Big/ \int_{L_{min}}^{K_{max}} \left[D L + \sqrt{3} D^2/4\right] n(L)\, dL \quad (5.27)$$

Where D is the width of an ice crystal. The $\left[D L + \sqrt{3} D^2/4\right]$ in the denominator of equation (5.27) is proportional to the surface area of a hexagon ice crystal, and ($D^2 L$) in the numerator is proportional to its volume. For scattering and absorption calculations, the ice crystal size is discretized into 30 bins, and the aspect ratio. D/L, used for the calculation is,

$$D/L = 1.00 \quad if \;\; 0 < L \leq 30\mu m$$

$$D/L = 0.80 \quad if \;\; 30 < L \leq 80\mu m$$

$$D/L = 0.50 \quad if \;\; 80 < L \leq 200\mu m$$

$$D/L = 0.34 \quad if \;\; 200 < L \leq 500\mu m$$

$$D/L = 0.22 \quad if \;\; L > 500\mu m$$

Which roughly corresponds to the observations.

The solar radiative properties of ice cloud are parameterized as a function of IWC and D_{ge}. More generally, it is assumed as (Fu 1996),

$$\beta = IWC\,(a_0 + a_1/D_{ge}) \quad (5.28a)$$

$$1 - \omega = b_0 + b_1 D_{ge} + b_2 D_{ge}^2 + b_3 D_{ge}^3 \quad (5.28b)$$

$$g = c_0 + c_1 D_{ge} + c_2 D_{ge}^2 + c_3 D_{ge}^3 \quad (5.28c)$$

Where the coefficients are obtained by numerical fitting to the single scattering properties computed from an “exact” light scattering and absorption program. The ice density ρ_i of 0.9167 $g\ cm^{-3}$ is used. The coefficients are given by Fu (1996) for a variety of spectrum bands.

The infrared radiative properties of ice cloud are parameterized in terms of IWC and D_{ge} as,

$$\beta = IWC\,(a_0 + a_1/D_{ge} + a_2/D_{ge}^2) \quad (5.29a)$$

$$\beta_a = \frac{IWC}{D_{ge}}\,(b_0 + b_1 D_{ge} + b_2 D_{ge}^2 + b_3 D_{ge}^3) \quad (5.29b)$$

$$g = c_0 + c_1 D_{ge} + c_2 D_{ge}^2 + c_3 D_{ge}^3 \quad (5.29c)$$

The single scattering albedo (ω) is calculated from,

$$1 - \omega = \beta_a/\beta \quad (5.30)$$

Using the composite light scattering and absorption scheme, the single scattering properties of cirrus clouds are derived at 36 wavelengths from 4 to 100 μm. The coefficients are obtained by numerical fitting to the single scattering properties computed from the composite scheme for 28 ice crystal size distributions. These coefficient values are given by Fu et al. (1998) for a variety of infrared spectrum bands.

Based on the works of Fu (1996) and Heymsfield and McFarquhar (1996), we can obtain the relationship between generalized effective size (D_{ge}) and effective radius (r_{ei}) of the ice crystals as,

$$D_{ge} = 1.0315\, r_{ei} \quad (5.31)$$

The coefficient is an updated value.

The effective radius of ice crystals (r_{ei}) is calculated based on Heymsfield and McFarquhar (1996) as a function of temperature and IWC,

$$r_{ei} = (1250/9.917) \cdot IWC^{0.109} \quad if \quad (T - 273.16) < -50 \quad (5.32a)$$

$$r_{ei} = (1250/9.337) \cdot IWC^{0.08} \quad if \quad -50 \le (T - 273.16) < -40 \quad (5.32b)$$

$$r_{ei} = (1250/9.208) \cdot IWC^{0.055} \quad if \quad -40 \le (T - 273.16) < -30 \quad (5.32c)$$

$$r_{ei} = (1250/9.387) \cdot IWC^{0.031} \quad if \quad -30 \le (T - 273.16) \quad (5.32d)$$

For GFDL microphysics, the calculation are as follows: first using equation (5.32) to calculate the effective radius (r_{ei}) for ice cloud, then convert it to the generalized effective size (D_{ge}) using equation (5.31), and finally obtained the optical properties of the ice cloud using equations (5.28) and (5.29).

For Thompson and WSM6 microphysics schemes, the effective radius for ice crystals and snow are calculated in the microphysics schemes. The ice water path is calculated using equation (5.24), and the snow water path is calculated by summing the snow water path and graupel water path.

For The Morrison-Gettelman microphysics scheme (MG3) (Morrison and Gettelman 2008, 2015; Gettelman et al. 2019), the effective radii for liquid cloud water, rain water, ice cloud and snowflakes are calculated in the MG3 microphysics scheme. The liquid water cloud path, rain water path, ice cloud water path and snow water path are calculated similarly to those in the Thompson and WSM6 microphysics schemes.

In summary, if the microphysics scheme has calculated the effective radii of the liquid water cloud, rain water, ice cloud and snowflakes, those effective radii can be passed to the cloud scheme and be used to calculate the optical properties of the cloud and precipitate. If there is no effective radius passed to the cloud scheme, the effective radius will be parameterized similarly to those used for the GFDL microphysics scheme.

5.4 Aerosol optics

Aerosols are usually a combined mixture of particles of different sources. Different components have different optical properties and relative humidity dependency. The operational GFS model uses a globally distributed aerosol data set OPAC (Optical Properties of Aerosols and Clouds) with horizontal resolution of five-degrees longitude-latitude (Hess et al 1998). A new global aerosol data set MERRA-2 (which is discussed in section 7.2) is currently under tests in GFS and may become operational in the future.

In the OPAC aerosol data set, climatological data of aerosol components are given at each geographic location (a five-degree grid area), including the aerosol profile type, the mixing ratios of the aerosol components, the mean particle number density, and the optical properties of each aerosol component. Seven typical vertical distribution profiles are specified. For each of the profiles chosen (based on different geographic location), up to five distinct vertical atmospheric domains are given, and up to ten different types of aerosol components are used to construct the aerosol profile. Based on the source of their origin, the ten types of aerosols (Koepke et al 1997 table 1; or Hou et al 2002 table 4) are divided into two groups. The first group includes six aerosol types, and their optical properties are not

sensitive to the atmospheric humidity. The coefficients for the first group of aerosol components are given by Hess et al. (1998). The second group contains four aerosol types. Those aerosols may absorb water content in the atmosphere. To account for variations of optical properties of these aerosols due to the changing of ambient relative humidity, a simple parameterization is given as (Hess et al. 1998),

$$\delta_{\upsilon,i} = a_{0\upsilon,j} + a_{1\upsilon,j} R_0 + a_{2\upsilon,j} R_1 \quad (5.33a)$$

$$\sigma_{\upsilon,i} = b_{0\upsilon,j} + b_{1\upsilon,j} R_0 + b_{2\upsilon,j} R_1 \quad (5.33b)$$

$$\omega_{\upsilon,i} = c_{0\upsilon,j} + c_{1\upsilon,j} R_0 + c_{2\upsilon,j} R_1 \quad (5.33c)$$

$$g_{\upsilon,i} = d_{0\upsilon,j} + d_{1\upsilon,j} R_0 + d_{2\upsilon,j} R_1 \quad (5.33d)$$

Where

$$R_0 = RH - 0.5$$

$$R_1 = exp\,(\gamma_{\upsilon,j} R_0)$$

$$R_2 = R_0^2$$

Values of a, b, and c and γ are specified. RH denotes the atmospheric relative humidity.

From the lower troposphere, up to the middle of the stratosphere, aerosol types, number concentrations, and radiative properties are specified. No traceable aerosol exists in the upper stratosphere. Up to five different types of aerosol components (out of a total of 10 distinct types) are given for each of the five-degree geographic locations. The effective optical properties of the aerosol mixture can be expressed as (Hou et al. 2002),

$$\delta_\upsilon = \overline{N} \sum c_i \delta_{\upsilon i} \quad (5.34a)$$

$$\omega_\upsilon = \sum c_i \omega_{\upsilon i} \delta_{\upsilon i} / \sum c_i \delta_{\upsilon i} \quad (5.34b)$$

$$g_\upsilon = \sum c_i g_{\upsilon i} \sigma_{\upsilon i} / \sum c_i \sigma_{\upsilon i} \quad (5.34c)$$

Where c_i is the mixing ratio of the i^{th} aerosol component, δ_{vi}, $\sigma_{\upsilon i}$, $\omega_{\upsilon i}$, and $g_{\upsilon i}$ are coefficients for extinction, scattering, single scattering albedo, and asymmetry factor, respectively, for a spectral band υ. $\overline{N}$ is the climatological mean value of aerosol particle number density in the domain.

The optical depth of aerosol of each model vertical layer is then readily defined as,

$$\tau_{\upsilon,k} = \delta_{\upsilon,k} H \left(e^{-z_{k+1}/H} - e^{-z_k/H}\right) \qquad if\ H \geq 0 \qquad (5.35a)$$

$$\tau_{\upsilon,k} = \delta_{\upsilon,k} \Delta z_k \qquad otherwise \qquad (5.35b)$$

Where H is the scale height of aerosols, z_k and Δz_k are height of the k^{th} model level and layer thickness in km, respectively.

$$\Delta z_k = H_{0k} \left[ln(p_{k+1/2}) - ln(p_{k-1/2}) \right] \qquad (5.36)$$

Where H_{0k} is the k^{th} layer's mean atmospheric scale height in km computed by model's hydrostatic equation, $p_{k+1/2}$ and $p_{k+1/2}$ are the pressure at the interfaces of layer *k*.

5.5 Gas optics

The shortwave and longwave radiative transfer can be accurately calculated by high spectral resolution line-by-line models such as LBLRTM (Clough et al. 1992). Depending on the number of spectral intervals, the cost of the computation can be enormous. Therefore, most of the GCM models are using the K-distribution method in recent years. GFS using RRTMG for the radiative transfer calculations (discussed in section 6). In RRTMG, the correlated k-distribution method is used. The shortwave and longwave regions are split into a number of bands. The gas absorptions are reordered within each band from the least to the most absorbing, as a function of the new coordinate, *g*, that varies from 0 (least absorbing) to 1 (most absorbing). The smooth absorption distribution versus *g* is then discretized by a handful of g-point, and each g-point is treated as monochromatic by the other parts of the radiation scheme.

In RRTMG, all gas, aerosols and cloud modules must use the same spectral discretization. Therefore, we need to ensure that the aerosol and cloud optical modules load the scattering data files with a matching spectral discretization.

6. RRTM, RRTMG and RRTMGP Radiative Transfer Models

The Rapid Radiative Transfer Model (RRTM) calculates shortwave fluxes, longwave fluxes and cooling rates for applications to general studies of the atmospheric radiative transfer and for implementation into GCMs (Mlawer et al. 1997). The correlated-*k* method was selected by RRTM for its computational efficiency with accuracy consistent with line-by-line radiative transfer models (LBLRTM) (Clough et al. 1992), and its direct adaptability to multiple-scattering calculations. RRTM carefully selects the band structure to handle various major (key-species) and minor absorbers, and uses two pressure regions for optimal treatment of various species. RRTM has been extensively validated against LBLRTM as well as against measurements. Based on the validation results, an accelerated version of the RRTM (RRTMG) has been produced for GCMs. RRTMG shares the same basic physics and absorption coefficients as RRTM, but it incorporates several modifications that improve computational efficiency and represent subgrid-scale cloud variability (Mlawer et al. 2016). In particular, the total number of quadrature points (g-points) used to calculate radiance in the longwave was reduced from 256 in RRTM_LW to 140 in RRTMG_LW. In the shortwave, the number of g-points was reduced from 224 in RRTM_SW to 112 in RRTMG_SW. In addition, the multiple scattering code DISORT employed by RRTM_SW was replaced with a much faster two-stream radiative transfer solver (Oreopoulos and Barker 1999) in RRTMG_SW. The McICA approach is used in RRTMG to address the complexity of representing fractional cloudiness in the presence of multiple scattering. The McICA is a statistical technique for representing subgrid-scale cloud variability including cloud overlap (Pincus et al. 2003).

6.1 The *k*-distributions and the correlated-*k* method

The *k*-distribution method for the computation of radiative transfer is based on the grouping of gaseous spectral transmittances according to the absorption coefficients k_{υ}(Liou 1992). In a homogeneous atmosphere, spectral transmittance is independent of the ordering of *k* for a given spectral interval. Hence, the wavenumber integration may be replaced by an integration over the *k* space. Assume the normalized probability distribution function for k_{v} in the interval $\Delta\upsilon$ is given by *f(k)*, and let the maximum and minimum absorption coefficients with $\Delta\upsilon$ be k_{max} and k_{min}, respectively, then the spectral transmittance may be expressed by,

$$\bar{T}_{\upsilon}(u) = \int_{\Delta\upsilon} e^{-k_{v}u}\,\frac{d\upsilon}{\Delta\upsilon} = \int_{0}^{\infty} e^{-k\,u}\,f(k)\,dk \qquad (6.1)$$

Where we have set $k_{max} = \infty$ and $k_{min} = 0$ for mathematical convenience, and u is the path length ($g\ cm^{-2}$) from absorbing gases and is defined as,

$$u(z) = \int_0^z \rho_a(z')\, dz'$$

And ρ_a denotes the density of the absorbing gas. We may further define a cumulative probability function in the form,

$$g(k) = \int_0^k f(k)\, dk \qquad (6.2)$$

Where $g(0) = 0$, $g(k \to \infty) = 1$, and $dg(k) = f(k)\, dk$. By definition, $g(k)$ is a monotonically increasing and smooth function in *k*-space, and therefore *k(g)* is also a smooth function in *g*-space. Using the *g*-function, the spectral transmittance can be written as,

$$T_{\upsilon}(u) = \int_0^1 e^{-k(g)\,u}\, dg \approx \sum_{j=1}^{M} e^{-k(g_j)\,u}\, \Delta g_j \qquad (6.3)$$

Therefore, the line-by-line (wave number) integration can be evaluated by a finite sum of exponential terms, as shown in equation (6.3).

The correlated-*k* method (or correlated *k*-distribution method) is an extension of the k-distribution method to nonhomogeneous paths first proposed by Lacis et al. (1979). In this method, the vertical nonhomogeneity of the atmosphere is accurately accounted for by assuming a simple correlation of k-distribution at different temperature and pressure. It is assumed that 1) the absorption coefficients at two wavenumbers, v_i and v_j ($i \neq j$), are the same at any arbitrary pressure and temperature, if they are the same at a reference pressure and temperature, 2) the ordering of the absorption coefficient with respect to its value is independence of pressure and temperature, and only one g exists for a given v at different levels.

Considering a nonhomogeneous atmosphere, the spectral-mean transmittance between two heights, z_1 and z_2, can be written in the form (Fu and Liou, 1992),

$$T_{\upsilon}(u) = \int_{\Delta v} exp\left[-\int_{z_1}^{z_2} k\,(v,p,T)\, \rho_a(z)\, dz \right] \frac{dv}{\Delta v} \qquad (6.4)$$

Under the assumptions 1) and 2) described above, Fu and Liou (1992) shows that equation (6.4) can be written as,

$$\bar{T}_{\upsilon}(u) = \int_0^1 exp\left[-\int_{z_1}^{z_2} k\,(g,p,T)\;\rho_a(z)\;dz\right]dg \qquad (6.5)$$

The method for calculating spectral-mean transmittance in a nonhomogeneous atmosphere based on equation (6.5) is referred to as the correlated k-distribution method (CKD).

Like the k-distribution method, the correlated-k method can be used for absorption bands in both solar and thermal infrared spectra and, at the same time, the results from this method can be directly incorporated into multiple-scattering processes associated with cloud and aerosol particles.

6.2 RRTMG_SW

RRTMG_SW contains 14 spectral bands (with 112 g-points) spanning a spectral wavenumber range of 820-50000 cm^{-1} (corresponding to a wavelength range 0.2-12.2 μm), each spectral band focuses on a specific set of atmospheric absorbing species as shown in Table 1.

Table 1. RRTMG-SW spectral bands and the corresponding absorbing species

Band #	Wavenumber Range	Number of g-points	Lower Atm (Key)	Lower Atm (Minor)	Mid/Up Atm (Key)	Mid/Up Atm (Minor)
16	2600-3250	6	H2O,CH4			
17	3250-4000	12	H2O,CO2		H2O,CO2	
18	4000-4650	8	H2O,CH4		CH4	
19	4650-5150	8	H2O,CO2		CO2	
20	5150-6150	10	H2O	CH4	H2O	CH4
21	6150-7700	10	H2O,CO2		H2O,CO2	
22	7700-8050	2	H2O,O2		O2	

23	8050-12850	10	H2O		—	
24	12850-16000	8	H2O,O2		O2	
25	16000-22650	6	H2O		—	
26	22650-29000	6	—		—	
27	29000-38000	8	O3		O3	
28	38000-50000	6	O3,O2		O3,O2	
29	820-2600	12	H2O		CO2	

As mentioned before, each g-point is treated in an equivalent manner as a spectral point is treated in a monochromatic radiative transfer method. All the radiative transfer theories and calculations discussed in sections 2 and 5 for shortwave radiation are valid. Scattering due to clouds greatly complicates the SW radiative transfer computations. To balance the trade-off between accuracy and speed, RRTMG-SW uses a two-stream approximation method with a delta-function adjustment. Several variations of the delta-adjustment two-stream methods are included in the GFS radiation transfer code; each holds its own strengths and shortcomings (King and Harshvadhan, 1986). The default (the same in operation runs) selection (iswmode=2) activates the Practical Improved Flux Method (PIFM) by Zdunkowski et al.(1980).

6.3 RRTMG_LW

RRTMG_LW contains 16 spectral bands (with 140 g-points) spanning a spectral wavenumber range of 10-3250 cm^{-1} (corresponding to a wavelength range 3.08-1000 μm), each spectral band focuses on a specific set of atmospheric absorbing species as shown in Table 2.

Table 2. RRTMG-LW spectral bands and the corresponding absorbing species

Band #	Wavenumber Range	Number of g points	Lower Atm (Key)	Lower Atm (Minor)	Mid/Up Atm (Key)	Mid/Up Atm (Minor)
1	10-350	8	H2O	N2	H2O	N2

2	350-500	14	H2O		H2O	
3	500-630	16	H2O,CO2	N2O	H2O,CO2	N2O
4	630-700	14	H2O,CO2		O3,CO2	
5	700-820	16	H2O,CO2	O3,CCL4	O3,CO2	CCL4
6	820-980	8	H2O	CO2		CFC11,CFC12
7	980-1080	12	H2O,O3	CO2	O3	CO2
8	1080-1180	8	H2O	CFC12,CFC22 CO2,O3,N2O	O3	CFC12,CFC22 CO2,N2O
9	1180-1390	12	H2O,CH4	N2O	CH4	N2O
10	1390-1480	6	H2O		H2O	
11	1480-1800	8	H2O	O2	H2O	O2
12	1800-2080	8	H2O			
13	2080-2250	4	H2O,N2O			O3
14	2250-2380	2	CO2		CO2	
15	2380-2600	2	N2O,CO2			
16	2600-3250	2	H2O,CH4		CH4	

RRTMG uses the absorption approximation (AA) for longwave radiative transfer calculation. Under the assumptions that (1) the Planck function varies linearly along the absorbing path in the layer and (2) the layer is homogeneous with respect to pressure, temperature, and species distribution with a characteristic absorption coefficient for the layer, the spectrally-averaged outgoing radiance from the atmosphere layer can be written as (Mlawer et al. 1997),

$$\overline{R}'_{\upsilon_1,\upsilon_2} = \frac{1}{\upsilon_2-\upsilon_1}\int_{\upsilon_1}^{\upsilon_2} d\upsilon\,[B^*(\upsilon,T_\upsilon)$$

$$+ \left[R_0(\upsilon) - B^*(\upsilon, T_\upsilon)\right] exp\left(- k(\upsilon, P, \theta) \frac{\rho \Delta z}{\mu_1}\right) \qquad (6.6)$$

Where υ_1 and υ_2 are the beginning and ending wavenumbers of the spectral interval, R_0 is the incoming radiance to the layer, $B^*(\upsilon, T_\upsilon)$ is an effective Planck function for the layer, T_υ is the transmittance for the layer , $k(\upsilon, P, \theta)$ is the absorption coefficient at layer with pressure *P* and temperature θ, and ρ is the absorber density.

Under the mapping $\upsilon \rightarrow g$, equation (6.6) becomes,

$$\overline{R}'_{\upsilon_1,\upsilon_2} = \int_0^1 dg \{B^*(g, T_g) + \left[R_0(g) - B^*(g, T_g)\right] exp\left(- k(g, P, \theta) \frac{\rho \Delta z}{\mu_1}\right)\} \qquad (6.7)$$

Where all the terms in equation (6.7) with dependence on υ has been transformed using the mapping $\upsilon \rightarrow g$. Despite the noncontinuous nature of the effective Planck function with respect to g, the smooth monotonically increasing behavior of the function *k(g)* can be achieved by partitioning the domain of the variable *g* into subintervals , each corresponding to a limited range of k(g) values, and determining a characteristic value k_j of the absorption coefficient for each subinterval. This characteristic value is used to compute the outgoing radiance for the entire subinterval. The resulting radiances, weighted by the sizes W_j of their respective subintervals ($\sum W_j = 1$), are summed to yield an approximation to the average radiance of equation (6.7):

$$\overline{R}'_{\upsilon_1,\upsilon_2} = \sum_j W_j R'_j = \sum_j W_j \left[B^*_j + (R_{0j} - B^*_j) exp\left(- k_j \frac{\rho \Delta z}{\mu_1}\right)\right] \qquad (6.8)$$

The only error introduced in the procedure is due to the use of single k_j, R_{0j} and B^*_j values for each subinterval instead of the full set of $k(\upsilon)$ and R_υ values. There is no error caused by the reordering procedure.

Similar to the band model discussed in section 4.2, the above method is extended to obtain the radiative transfer for vertically inhomogeneous atmosphere by dividing the atmosphere into layers, each layer is treated as described above, and using the outgoing radiance at each value of *g* as the incoming radiance for the same *g* value for the adjacent layer. This procedure treats each subinterval of *g* in an equivalent manner as a spectral point is treated in a monochromatic radiative transfer method. Under the condition that the *k* distribution in a given layer is fully correlated in spectral space with the *k* distribution in the next layer, the extension of this method to an inhomogeneous atmosphere is exact. However, In general the mapping $\upsilon \rightarrow g$ is not fully correlated between the adjacent layers, so the correlated-*k* method is only an approximate treatment of the radiative transfer for an inhomogeneous atmosphere.

6.4 RRTMGP

RRTMG radiation code was developed at AER ~ 20 years ago (funded by ARM 1995-2000). The FORTRAN code is written for CPUs, and has many conditional branches aimed at minimizing the number of floating-point operations. The code is also not effectively vectorized and is generous in its use of memory. The RRTMG is also less accurate and is based on out-of-date spectroscopy, and needs tuning occasionally.

RRTMGP ('P' stands for 'parallel') (Pincus et al, 2019) is a new version of the RRTMG radiation code. The RRTMGP is a high-performance broadband radiation code for the current generation of computational architectures. The RRTMGP code is completely re-written, and the new code consists of two related code bases: RTE and RRTMGP. RTE provides methods for solving a spectrally detailed radiative transfer problem; its complement, RRTMGP, determines the parameters (i.e, optical properties and source functions) of such a radiative transfer problem for the gaseous component of the atmosphere given the physical state and composition. RTE+RRTMGP is written in FORTRAN 2003, and many components are implemented as FORTRAN classes. Most of the calculation schemes are redesigned and rewritten for computation accuracy, efficiency, and flexibility in the parallel computation environment. RRTMGP code exhibits profound improvements in speed for GPU and vector CPU machines and lesser, but still valuable, speed-ups on other CPU-based platforms relative to the current version of the code.

RRTMGP code uses 16 bands for LW and 14 bands for SW (the band intervals are slightly different compared to those in RRTMG), with 16 g-points in each band (total 256 g-points for LW and 224 g-points for SW). In the RRTMGP code, the surface pressure is increased to 1096mb (from 1054mb in RRTMG), and the temperature range is expanded to 160-355K (from 160-340K in RRTMG), so the absorption coefficients are valid for more

extreme cases. RRTMGP also improves accuracy of the radiative flux calculations following the improvement of the LBLRTM based on the new spectroscopic knowledge.

Table 3 and Table 4 show the band structures used in the current version of RRTMGP for shortwave and longwave, respectively. The band values in the longwave differ modestly from those in RRTMG. The ordering of shortwave bands is strictly monotonic, abandoning the idiosyncratic ordering of RRTMG. Both changes imply that any fits, for example, for cloud optical properties made for RRTMG will need to be revisited before use in RRTMGP. For detailed information, the reader is referred to Pincus et al (2019).

Table 3. RRTMGP-SW spectral bands and the corresponding absorbing species

Band #	Wavenumber Range	Number of g points	Lower Atm (Key)	Lower Atm (Minor)	Mid/Up Atm (Key)	Mid/Up Atm (Minor)
1	820-2680	16	H2O,CO2	CH4,N2O,N2	H2O,CO2	CH4,N2O,O3
2	2680-3250	16	H2O,CH4		CH4	
3	3250-4000	16	H2O,CO2		H2O,CO2	
4	4000-4650	16	H2O,CH4		CH4	
5	4650-5150	16	H2O,CO2		CO2	
6	5150-6150	16	H2O	CH4	H2O	CH4
7	6150-7700	16	H2O	CO2	H2O,CO2	
8	7700-8050	16	H2O,O2		H2O,O2	
9	8050-12850	16	H2O	O2	H2O	O3
10	12850-16000	16	H2O,O2	O3	H2O,O2	O3
11	16000-22650	16	H2O	O3,O2,NO2	O3	O2,NO2
12	22650-29000	16	—	NO2	—	NO2
13	29000-38000	16	O3		O3	
14	38000-50000	16	O3,O2		O3,O2	

Table 4. RRTMGP-LW spectral bands and the corresponding absorbing species

Band #	Wavenumber Range	Number of g points	Lower Atm (Key)	Lower Atm (Minor)	Mid/Up Atm (Key)	Mid/Up Atm (Minor)
1	10-250	16	H2O	N2	H2O	N2
2	250-500	16	H2O		H2O	
3	500-630	16	H2O,CO2	N2O	H2O,CO2	N2O
4	630-700	16	H2O,CO2		O3,CO2	
5	700-820	16	H2O,CO2	O3,CCL4,CFC-22	O3,CO2	CCL4,CFC-22
6	820-980	16	H2O	CO2,CFC-11,CFC-12,HFC-143a	-----	CFC-11,CFC-12,HFC-143a
7	980-1080	16	H2O,O3	CO2	O3	CO2
8	1080-1180	16	H2O	CO2,O3,N2O,CFC-12,CFC-22,HFC-23,HFC-32,HFC-125,HFC-134a	O3	CO2,CO,CFC-12,CFC-22,HFC-23,HFC-32,HFC-125,HFC-134a
9	1180-1390	16	H2O,CH4	N2O,CF4,HFC-134a,HFC-143a	CH4	N2O,CF4,HFC-134a,HFC-143a
10	1390-1480	16	H2O		H2O	
11	1480-1800	16	H2O	O2	H2O	O2
12	1800-2080	16	H2O,CO2		-----	
13	2080-2250	16	H2O,N2O	CO2,CO	-----	O3
14	2250-2390	16	CO2		CO2	
15	2390-2680	16	H2O,CO2	N2O,N2	----	
16	2680-3250	16	H2O,CH4		CH4	

7. Climatology Data

The GFS model uses some climate fields that do not depend on initial conditions and forecast steps. Some of the fields need to be updated when new data is available. The section discusses where and how to obtain these climate data.

7.1 Astronomy data

Solar constant needs to be updated about every 11 years. Dr. Van den Dool kindly provided the solar constant update in 2005, 2011 and 2019. The following paragraph is written by Dr. Van den Dool:

The solar constant is updated based on a regression for the annual means solar constant S and sunspot number N,

S = a*N + b,

This relation predicts the solar constant from the sunspot number. The Total Solar Irradiance TSI (or S) data is downloaded from https://spot.colorado.edu/~koppg/TSI/ for 1750-2018 (2019 not yet available). These are annual S numbers. For the period 1979-2018, it is assumed that these are actually measurements by satellite (calibrated and calibrated some more). For 1979-2018 we also downloaded annual sunspot numbers (N) derived from http://sidc.oma.be/silso/datafiles . For 1979-2018 we then find S=0.004*N +1361 as regression with a modest 0.83 correlation. This regression is applied to the predicted sunspot number (N) out of SWPC (their latest update of the forecast for solar cycle 25 made in Dec 2019). This yields estimates of the solar constant S for 2019-2033. (This is a little farther out than 11 years since SWPC expects a very long next cycle of 13 rather than 11 years. The next cycle is also expected to be weak.) The result is given in the Table immediately below, as well as in the attached excel (in the manner NCO wants it).

Table: Annual solar constants with 1361W/m^2 subtracted. Along each row we have 10 years.

	+0	+1	+2	+3	+4	+5	+6	+7	+8	+9
1850	0.70	0.50	0.42	0.29	0.10	-0.02	-0.12	-0.05	0.19	0.48
1860	0.63	0.62	0.50	0.35	0.30	0.28	0.16	0.03	0.15	0.47
1870	0.68	0.97	0.73	0.63	0.34	0.01	-0.22	-0.28	-0.39	-0.41
1880	-0.24	0.09	0.15	0.11	0.32	0.22	0.06	-0.14	-0.19	-0.22
1890	-0.23	-0.12	0.17	0.35	0.47	0.34	0.23	-0.06	-0.11	-0.18
1900	-0.27	-0.36	-0.37	-0.28	0.01	0.00	0.24	0.13	0.15	0.02
1910	-0.08	-0.29	-0.34	-0.29	-0.21	0.10	0.41	0.57	0.78	0.46
1920	0.12	-0.11	-0.30	-0.40	-0.40	-0.30	0.04	0.31	0.24	0.10

1930	0.19	-0.05	-0.15	-0.16	-0.14	-0.02	0.44	0.72	0.67	0.63
1940	0.40	0.25	0.08	-0.09	-0.09	0.15	0.28	0.72	0.92	0.73
1950	0.62	0.19	0.11	0.03	-0.02	0.11	0.49	1.10	1.36	1.06
1960	0.93	0.58	0.19	0.01	-0.12	-0.17	-0.07	0.14	0.44	0.53
1970	0.41	0.24	0.19	0.07	-0.02	-0.04	-0.06	0.05	0.23	0.76
1980	0.69	0.71	0.42	0.39	-0.02	-0.16	-0.11	-0.03	0.28	0.74
1990	0.68	0.59	0.53	0.31	0.12	0.02	-0.10	0.08	0.47	0.73
2000	0.95	0.90	0.97	0.50	0.30	0.14	0.10	0.00	-0.02	-0.01
2010	0.23	0.46	0.59	0.61	0.59	0.70	0.34	0.21	0.26	0.04
2020	0.04	0.06	0.12	0.20	0.36	0.44	0.46	0.40	0.32	0.20
2030	0.12	0.08	0.06	0.04						

A few more comments from Dr. Van den Dool: (Dec 2019)

1) We have performed the tasks in 2005 and 2011, and now in 2019. The status of the data (calibration) and availability (daily, annual etc) were very different at these three moments in time. Some basic uncertainties remain, both about N and TSI, for a casual user and different outlets exist.

2) The regression relating N to S has become weaker when adding the data for 2011-2018, which was a very weak solar cycle. One must acknowledge that data from 3 or 4 solar cycles is very little, and this situation will improve only slowly. While the regression is based mainly on the quasi 11 year cycle, longer term changes enter the calculation. The last few years appear ‘anomalous’ by having near zero N, but not very low S.

3) We are ‘lucky’ to deal with this question at this time. Normally SWPC does not make forecasts for the next solar cycle until we are IN it. But on this occasion they made a forecast for cycle 25 while cycle 24 may not yet have quite ended. It is difficult to know, in real time, the exact moment when cycle M ends and cycle M+1 starts. The forecast for cycle 25 (or what remains of it) will be updated in the coming years, but a forecast for any year >= 2033 may not be given until well after 2030.

4) The numbers in the above Table for 2019-2033 need to be replaced when the observations become available, one for each year at some point in the next year. The new solar cycle 25 may give us surprises, so we should not rely on outdated values for the next many years. When someone takes a serious look at the observations X years from now we also cannot rule out that more calibration has taken place and this would change the whole Table back to 1850 or 1750.

7.2 Aerosol

As discussed in section 5.4, GFS operational model currently uses globally distributed aerosol data set OPAC, with horizontal resolution of five-degrees longitude-latitude (Hou et al. 2002). Their data set includes both winter and summer climatological values of aerosol distribution. At NCEP, the data set is interpolated to obtain monthly data with the same horizontal resolution.

The optical properties of the atmospheric aerosols are computed from the five-degree longitude-latitude data set (Hess et al. 1998; WMO WCP-112, 1986). Aerosol components and vertical profiles are specified based on geographic location, and then the effective optical properties of the aerosol mixture are calculated according to the aerosol components and vertical profile for each of the five degree geographic locations.

A new global aerosol data set MERRA-2 (the Modern-Era Retrospective Analysis for Research and Applications, version 2) (Buchard et al 2017, Randles et al 2017) is added to the global model as an alternative aerosol data set (Cheng and Yang, 2023). This new aerosol data has been tested and evaluated and will be included in the GFS for the upcoming operational implementation. MERRA-2 is a global atmospheric reanalysis produced by the NASA Global Modeling and Assimilation Office (GMAO). It spans the satellite observing era from 1980 to the present. The MERRA-2 data has high spatial (½° latitude by ⅝° longitude and 72 model levels extending up to 1 hPa) and temporal (hourly) resolutions. The climatology MERRA-2 data used by the GFS are monthly means averaged from 2003 to 2014. Both the monthly averaged MERRA2 aerosol dataset and the associated aerosol optical properties look-up-tables (LUTs) are provided by NASA GSFC.

The MERRA-2 data can be obtained from website:

https://climatedataguide.ucar.edu/climate-data/nasas-merra2-reanalysis

7.3 Greenhouse gasses

Concentrations of atmospheric greenhouse gasses are either obtained from global network measurements, such as carbon dioxide (CO_2), or taking the climatological constants, such as methane, nitrous oxide, oxygen, and CFCs, etc. In the operational GFS, the actual CO_2 value for the forecast time is an estimation based on the most recent 3-year observations. In the lower atmosphere (< 3km) a monthly mean CO_2 distribution in 15 degree

horizontal resolution is used, while a global mean monthly value is used in the upper atmosphere.

Starting from 2018, the CO_2 data is downloaded from the World Data Center for Greenhouse Gases (WDCGG). WDCGG is a World Data Centre (WDC) operated by the Japan Meteorological Agency (JMA) under the Global Atmosphere Watch (GAW) programme of the World Meteorological Organization (WMO). WDCGG collects, archives and distributes data provided by contributors on greenhouse gasses (such as CO_2, CH_4, CFCs, N_2O) and related gasses (such as CO) in the atmosphere and elsewhere.

The web site: https://gaw.kishou.go.jp/

a) prior to 2018 NCEP data were collected from the following web sources (discontinued):

Global Atmosphere Watch (GAW)

- http://gaw.kishou.go.jp (old site)
- http://ds.data.jma.go.jp/gmd/wdcgg/ (new)

b) additional sources used in early time, including data extracted from the ice core to obtain CO_2 concentration prior 1957. Data from those sources have a different format than the main data center (GAW) and need to process manually.

Note some of the website might not be accessible anymore, so some of old data sources might be lost, thus the previously processed 2-d CO_2 data in the directory co2dat_4a might not be reproducible.

DOE / Carbon Dioxide Information Analysis Center (CDIAC)

- http://cdiac.ornl.gov

NOAA / Climate Monitoring and Diagnostics Laboratory (CMDL)

- http://www.cmdl.noaa.gov

The downloaded data is processed, and three gridded monthly data sets (15 degree horizontal resolution) are created to use in the NCEP NWP models. For example, we created three new CO_2 data files in October 2022. The three CO_2 data files are: 1) The 2021 CO_2 data set (file name: global_co2historicaldata_2021.txt). This new data file is created (and replaces the old 2021 updated CO_2 file) since we have all the CO_2 data for 2021. 2) Updated 2022 CO_2 data set (file name: global_co2historicaldata_2022.txt_proj_u). This data is created (and replaces the old projected 2022 CO_2 file) based on previous year CO_2 data and part of the current year CO_2 data. 3) The 2023 projected data set (file name: global_co2historicaldata_2023.txt_proj). This new data set is projected based on the 2021 and 2022 observed CO_2 data.

7.4 Surface albedo

Surface spectral albedos for direct and diffuse radiation are needed for the radiation transfer calculation. In addition, the surface energy balance equation needs the spectrally integrated direct+diffuse albedo. In operational GFS, the Noah LSM is used. In a given model grid, the area is divided into three possible fractions: ice cover which includes snow and sea ice, open water, and land area without snow covering. The albedos for ice cover and open water are parameterized based on zenith angle, surface temperature, orographic height, snow depth, and surface roughness. The surface albedo for land is derived from the Moderate Resolution Imaging Spectroradiometer (MODIS) instrument (Wang et al., 2014), and modified based on zenith angle and snow cover. The final total surface albedo is calculated based on the fraction coverage of the land, open water and ice fractions (Yang et al. 2008).

In recent years, the Noah Multi-Parameterization (Noah-MP) model (Niu et al. 2011, Yang et al. 2011) is used for the next generation of Noah LSM development. The Noah-MP includes the calculation of albedo as a function of radiation transport within the canopy. A two-stream formulation for solar radiation exchange within the plant canopy is used in Noah-MP, which computes the surface albedo as a function of the solar elevation, diffuse and direct solar radiation, vegetation properties, and bare soil/ground albedo. The overall ground albedos of the direct and diffuse radiation are weighted as a function of “soil” and snow albedos. There are detailed descriptions of the Noah-MP model in the NCAR technical report (He et al. 2023).

8. Input to the Radiation Scheme

As described in previous sections, the RRTM radiation contains several components (data and processes) for SW and LW calculation. In the radiation initialization stage, several items need to be defined to properly execute the model. It includes essential input data and parameters (radiation and cloud microphysics) for the choice of schemes.

The essential input data for radiation initialization are,

a. solar constant (7.1)

b. global aerosol data (7.2)

c. global CO_2 data (7.3)

d. global O_3 data (from data analysis)

e. global surface emissivity data (7.4)

Because each cloud microphysics scheme has its unique hydrometers (contents and size), in order to properly process the SW and LW, the parameters need to be defined. There are also other major parameters that involve the universal process of cloud information, cloud overlapping, sub-column cloud approximation, cloud condensate amount vertical smoothing, cloud condensate horizontally normalization, and vertical direction index.

Following the CCPP (The Common Community Physics Package) metadata input table for LW and SW main programs, the following data must be provided to the GFS RRTMG subroutines,

Pressure at full and half levels.
Temperature at full and half levels.
Water vapor (specific humidity) at half levels.
Volume mixing ratios for the following gasses: O_3, CO_2, N_2O, CH_4, O_2, CO, CFC11, CFC12, CCL4.
Aerosol optical depth, single scattering albedo, and asymmetry parameter.
Surface albedo and emissivity.
Surface ground temperature for longwave radiation.
Cosine of the Solar zenith angle.
Solar constant.
Seeds to generate random numbers for shortwave and longwave radiation calculation.
Horizontal cloud fraction of the grid box.
Cloud optical properties which includes the following: 1) cloud optical depth for some selected band; 2) cloud liquid water path, cloud ice water path, cloud rain water path, cloud snow water path; 3) mean effective radii for liquid water cloud, ice cloud, raindrops and snowflakes.

The cloud optical properties are optional. For detailed input/output of the GFS RRTMG radiation schemes, the reader is referred to DTC CCPP documentation (or GFS RRTMG longwave/shortwave radiation FORTRAN code).

9. FORTRAN Code Structure of the GFS Radiation Scheme

The GFS radiation package consists of two core radiative transfer models (LW and SW) plus five supporting modules (gasses, clouds, aerosols, astronomy, and surface). This structure is designed to work efficiently, and the radiation scheme connects easily with the model dynamics and various model physics processes. With a standard 3-part core radiation module structure (i.e. parameters, data, and main procedures) as well as setting up a unified input/output argument list, different radiation core models (e.g. GFDL, NASA, and AER's RRTM/RRTMG, etc.) can be easily switched without code modifications to the other parts of the model. The five supporting modules provide safer places for reduced coding error, and easily locating and upgrading particular algorithms, as well as connecting smoothly with external physics processes. Program coding, however, was selected at the halfway of the standard FORTRAN-77 and modern FORTRAN-9x, due to the continuing evolution of the program language at the time and different acceptance stages on different machine compilers. As the modern coding standards become prevailing now, a new generation of radiation core models, such as RTE-RRTMGP, has been developed by AER/WU. And a further revision of the package's overall structure would be preferred to better fit into the modern numerical computation environment.

The GFS radiation module structure (copied from online CCPP scientific document, version 2.0: https://dtcenter.ucar.edu/gmtb/users/ccpp/docs/sci_doc_v2/GFS_RRTMG.html) is shown below,

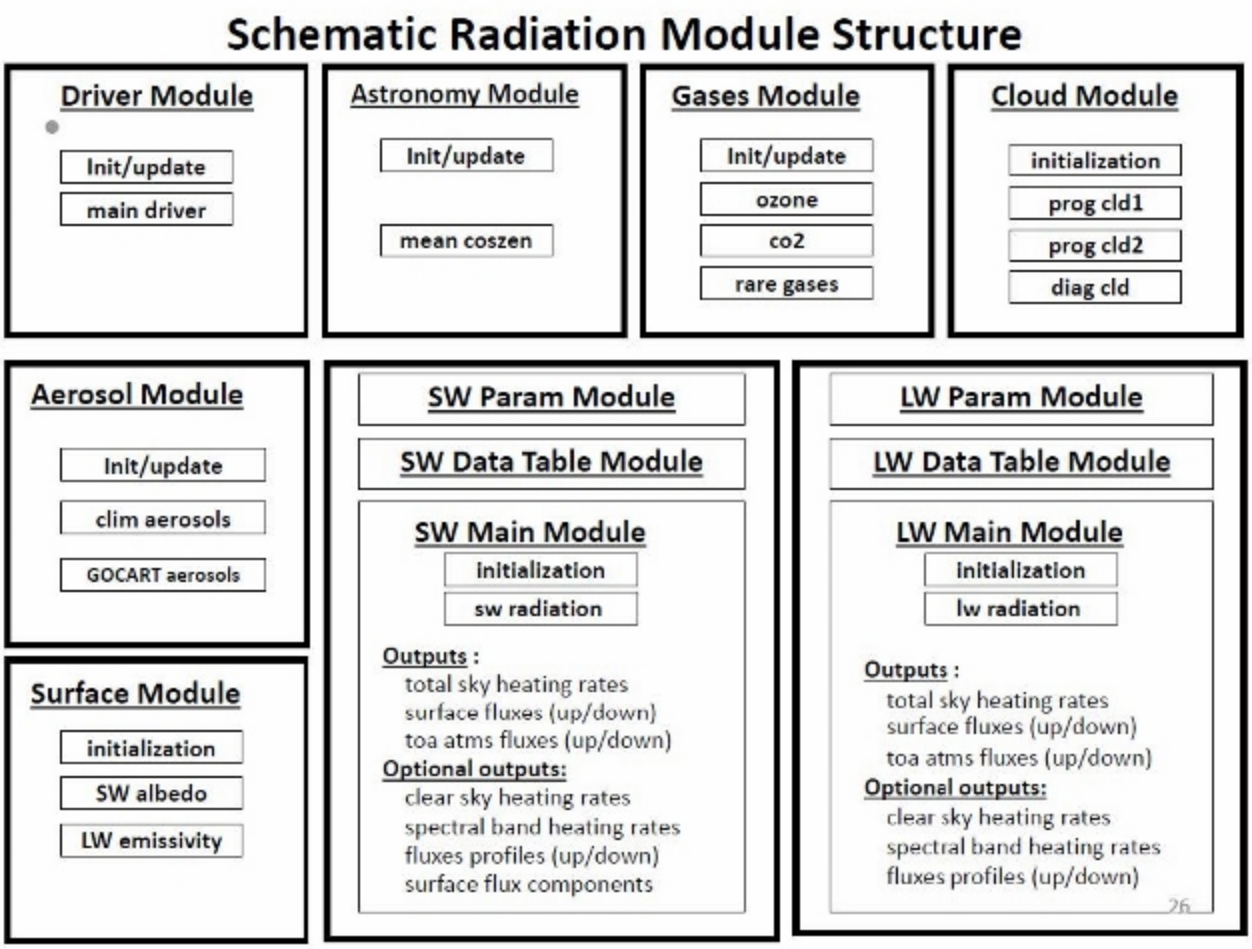

The radiation flowchart based on CCPP is shown in the next page, only the major subroutines/functions are listed in the flowcharts. The CCPP physics will be used in current and future GFS implementations.

Acknowledgements: The authors would like to thank Anning Cheng, Zhichang Guo, Yu-Tai Hou, Quanhua Liu and Helin Wei for reviewing the draft and giving suggestions and comments. The first author would also like to thank Jack Kain (NSSL) for giving the opportunity to work on the GFS radiation scheme.

Flowchart of the GFS radiation scheme based on CCPP

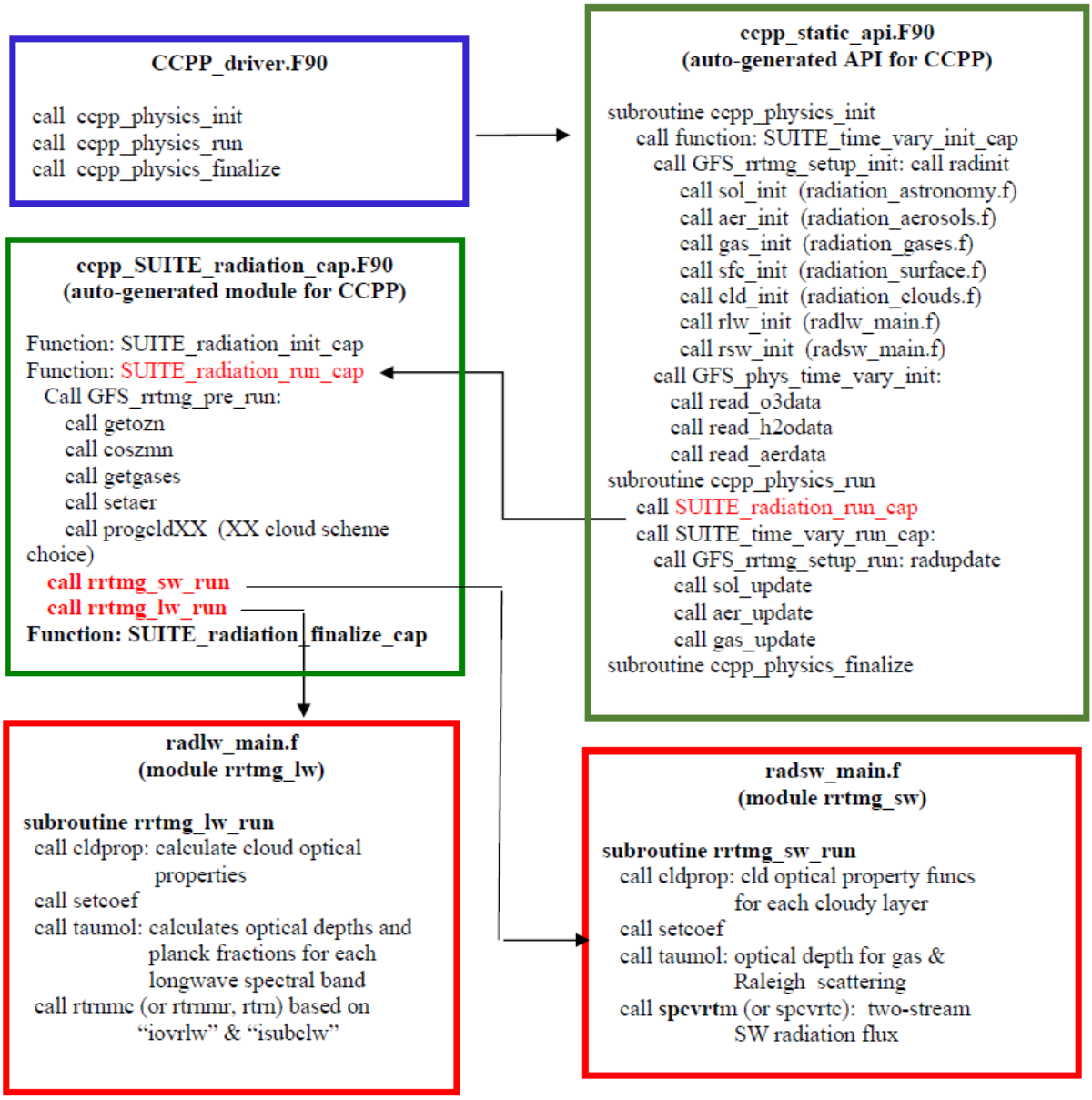

REFERENCES

Barker, H. W., G. L. Stephens, and Q. Fu, 1999: The sensitivity of domain averaged solar fluxes to assumptions about cloud geometry, *Q. J. R. Meteorol. Soc*., 125, 2127 – 2152.

Bergman, J. W., and P. J. Rasch, 2002: Parameterizing vertically coherent cloud distributions. *J. Atmos. Sci.*, 59, 2165–2182.

Briegleb, B. P., 1992: Delta-Eddington approximation for solar radiation in the NCAR community climate model. *Journal Of Geophysical Research-Atmospheres*, *97*, 7603-7612.

Briegleb, B. P., Minnis, P., Ramanathan, V., & Harrison, E., 1986: Comparison of regional clear-sky albedos inferred from satellite-observations and model computations. *Journal Of Climate And Applied Meteorology*, *25*, 214-226.

Buchard, V., Randles C.A., da Silva, A.M., Darmenov, A., Colarco, P. R., Govindaraju, R., Ferrare, R., Hair, J., Beyersdorf, A. J., Ziemba, L. D., and Yu, H., 2017: The MERRA-2 Aerosol Reanalysis, 1980 - Onward, Part II: Evaluation and Case Studies. *J. Climate*, 30, 6851–6872.

Cahalan, R. F., W. Ridgway, W. J. Wiscombe, T. L. Bell, and J. B. Snider, 1994: The albedo of fractal stratocumulus clouds. *J. Atmos. Sci.*, 51, 2434–2455.

Chen, J.-H and S.-J Lin, 2011: The remarkable predictability of inter-annual variability of Atlantic hurricanes during the past decade. *Geophysical Research Letters*, 38(L11804):6, 2011.

Chen, J.-H and S-J. Lin, 2013: Seasonal predictions of tropical cyclones using a 25-km-resolution general circulation model. *J. Climate*, 26(2):380–398.

Cheng, A. and F. Yang: Direct radiative effects of aerosols on numerical weather forecast – a comparison of two aerosol datasets in the NCEP GFS. *Weather and Forecasting*, DOI 10.1175/WAF-D-22-0060.1.

Chou, M-D, 1992: A solar radiation model for use in climate studies. *J. Atmos. Sci.*, 49, 762-772.

Chou, M.-D. and Suarez, M.J., 1999: A Solar Radiation Parameterization (CLIRAD-SW) Developed at Goddard Climate and Radiation Branch for Atmospheric Studies. *NASA Technical Memorandum NASA/TM-1999-104606*

Clough, S. A., M. J. Iacono, and J.-L. Moncet, 1992: Line-by-line calculation of atmospheric fluxes and cooling rates: Application to water vapor. *J. Geophys. Res.,* 97, 15761–15785.

Clough, S.A., and M.J. Iacono, 1995: Line-by-line calculations of atmospheric fluxes and cooling rates II: Application to carbon dioxide, ozone, methane, nitrous oxide, and the halocarbons. *J. Geophys. Res.*, 100, 16,519-16,535.

Elsasser, W. M., 1942: Heat transfer by infrared radiation in the atmosphere, *Harvard Meteorological Studies No. 6*, Harvard University Press.

Fu, Q., and K. N. Liou, 1992: On the correlated k-distribution method for radiative transfer in nonhomogeneous atmospheres. *J. Atmos. Sci.*, 49, 2139–2156.

Fu, Q., 1996: An accurate parameterization of the solar radiative properties of cirrus clouds for climate models. *J. Climate,* **9,** 2058–2082.

Fu, Q., P. Yang, and W. B. Sun, 1998: An accurate parameterization of the infrared radiative properties of cirrus clouds for climate models *J. Climate*, 11, 2223–2237.

Geleyn J-F, Hollingsworth A. 1979. An economical analytical method for the computation of the interaction between scattering and line absorption of radiation. *Contrib. Atmos. Phys.* 52: 1–16.

Gettelman A. and H. Morrison, 2015: Advanced two-moment bulk microphysics for global models. part i: Off-line tests and comparison with other schemes. *Journal of Climate*, 28(3):1268–1287.

Gettelman A., H. Morrison, K. Thayer-Calder, and C. M. Zarzycki, 2019: The impact of rimed ice hydrometeors on global and regional climate. *Journal of Advances in Modeling Earth Systems*.

Goody, R., West, R., Chen, L., & Crisp, D. 1989: The correlated-k method for radiation calculations in nonhomogeneous atmospheres. *J. Quant. Spectr. Rad. Transf.*, 42, 539-550.

He, C., P. Valayamkunnath, M. Barlage, F. Chen, D. Gochis, R. Cabell, T. Schneider, R. Rasmussen, G.-Y. Niu, Z.-L. Yang, D. Niyogi, and M. Ek 2023: *The Community Noah-MP Land Surface Modeling System Technical Description (Version 5.0)*

Hess, M., Koepke, P., & Schult, I., 1998: Optical properties of aerosols and clouds: the software package OPAC, *Bulletin of the American Meteorological Society*, Vol. 79, No. 5, p. 831-844.

Hogan, R. J., and A. J. Illingworth, 2000: Deriving cloud overlap statistics from radar,*Q. J. R. Meteorol. Soc.*,126, 2903–2909.

Hong S. Y. and J. J. O. Lim, 2006: “The WRF single-moment 6-class microphysics scheme (WSM6),” *Journal of the Korean Meteorological Society*, vol. 42, pp. 129–151.

Hou, Y.-T., S. Moorthi, and K.A. Campana, 2002: Parameterization of solar radiation transfer in the NCEP models. *NCEP Office Note 441*.

Hu, Y., and K. Stamnes, 1993: An accurate parameterization of the radiative properties of water clouds suitable for use in climate models. *J. Climate,* 6, 728–742.

King, M. D. and Harshvardhan 1986: Comparative accuracy of selected multiple scattering approximations. *J. Atmos. Sci.,* 43, 784–801.

Koepke, P., M. Hess, I. Schult, and E. P. Shettle, 1997: Global Aerosol Data Set. *MPI Meteorologie Hamburg Report No. 243*, 44 pp.

Lacis, A., W. C. Wang, and J. Hansen. 1979: Correlated k-distribution method for radiative transfer in climate models: *Application to effect of cirrus clouds on climate,* NASA Conf. Publ., 2076, 309-314.

Lacis, A.A.; Oinas, V. A, 1991: Description of the correlated k-distribution method for modeling nongray gaseous absorption, thermal emission, and multiple-scattering in vertically inhomogeneous atmospheres. *J. Geophys. Res.*, *96*, 9027–9063.

Li, J., 2000: Gaussian quadrature and its application to infrared radiation. *J. Atmos. Sci*., 57, 753–765.

Lin Y.-L., R. D. Farley, and H. D. Orville, 1983: Bulk parameterization of the snow field in a cloud model. *J. Climate Appl. Meteor.*, 22:1065–1092.

Liou, K. N., 1973: A numerical experiment on Chandrasekhar's discrete-ordinates method for radiative transfer: Application to cloudy and hazy atmospheres. *J. Atmos. Sci. 30*, 1303–1326.

Liou, K. N., 1974: On the radiative properties of cirrus in the window region and their influence on remote sensing of the atmosphere, *J. Atmos. Sci.* 31, 522–532.

Liou, K.N., 1992: Radiation and Cloud Processes in the Atmosphere, Oxford University Press, 487pp.

Liou, K.N., 2002: *An Introduction to Atmospheric Radiation*, Second Edition, Academic Press, 577pp.

Meador, W.E., and W.R. Weaver, 1980: Two-Stream Approximations to Radiative Transfer in Planetary Atmospheres: A Unified Description of Existing Methods and a New Improvement, 37, *J. Atmos. Sci.*, 630–643.

Mlawer, E. J., and S. A. Clough, 1998: Shortwave and longwave enhancements in the rapid radiative transfer model. Proc. Seventh Atmospheric Radiation Measurement (ARM) Science Team Meeting, San Antonio, TX, U.S. Dept. of Energy, 409– 413

Mlawer, E.J., M.J. Iacono, R. Pincus, H.W. Barker, L. Oreopoulos and D.L. Mitchell 2016: Contributions of the ARM Program to Radiative Transfer Modeling for Climate and Weather Applications, The Atmospheric Radiation Measurement Program: The First 20 Years, Meteor. Monograph, **57**, *Amer. Meteor. Soc.*.

Mlawer, E.J., S. J. Taubman, P. D. Brown, M. J. Iacono, and S. A. Clough, 1997: Radiative transfer for inhomogeneous atmospheres: RRTM, a validated correlated-k model for the longwave. J. Geophys. Res., 102, 16 663–16 682.

Morcrette, J. J., and Y. Fouquart, 1986: The overlapping of cloud layers in shortwave radiation parameterizations. *J. Atmos. Sci.*, 43, 321–328.

Morrison Hugh and Andrew Gettelman, 2008: A new two-moment bulk stratiform cloud microphysics scheme in the community atmosphere model, version 3 (cam3). part i: Description and numerical tests. *Journal of Climate*, 21(15):3642–3659.

Niu, G.-Y., et al. 2011: The community Noah land surface model with multiparameterization options (Noah-MP): 1. Model description and evaluation with local-scale measurements. *J. Geophys. Res.*, 116, D12109, doi: 10.1029/2010JD015139.

Oreopoulos, L., and H. W. Barker, 1999: Accounting for subgrid scale cloud variability in a multi-layer 1D solar radiative transfer algorithm. *Quart. J. Roy. Meteor. Soc.*, 125, 301–330.

Pincus, R., H. W. Barker, and J.-J. Morcrette, 2003: A fast, flexible, approximate technique for computing radiative transfer in inhomogeneous cloud fields. *J. Geophys. Res.*, 108, 4376.

Pincus R., E.J. Mlawer and J.S. Delamere, 2019: Balancing accuracy, efficiency, and flexibility in radiation calculations for dynamical models. *Journal of Advances in Modeling Earth Systems*, 11, 3074-3089.

Raisanen P., Barker H.W. 2004: Evaluation and optimization of sampling errors for the Monte Carlo independent column approximation. *Q. J. R. Meteorol. Soc.* 130: 2069–2086.

Randles, C. A., da Silva, A. M., Buchard, V., Colarco, P. R., Darmenov, A., Govindaraju, R., Smirnov, A., Holben, B., Ferrare, R., Hair, J., Shinozuka, Y., and Flynn, C. J., 2017: The MERRA-2 Aerosol Reanalysis, 1980 - Onward, Part I: System Description and Data Assimilation Evaluation. *J. Climate,* 30, 6823–6850.

Shonk, J. K. P., Hogan, R. J., Edwards, J. M. and Mace, G. G. 2010: Effect of improving representation of horizontal and vertical cloud structure on the Earth's global radiation budget. Part I: review and parametrization. *Quarterly Journal of the Royal Meteorological Society,* 136 (650). pp. 1191-1204. ISSN 1477-870X

Slingo, A., 1989: A GCM parameterization for the shortwave radiative properties of water clouds,*J. Atmos. Sci.*,46, 1419–1427.

Stamnes, K., S.-C. Tsay, W. Wiscombe and K. Jayaweera, 1988: Numerically stable algorithm for discrete-ordinate-method radiative transfer in multiple scattering and emitting layered media. *Appl. Opt.* 27, 2502-2509.

Stamnes K., S-C. Tsay, W. Wiscombe, and I. Laszlo, 2000: DISORT: A general purpose Fortran program for discrete-ordinate-method radiative transfer in scattering and emitting media. *Documentation of Methodology Report,* climate.gsfc.nasa.gov

Thompson Gregory, Roy M. Rasmussen, and Kevin Manning, 2004: Explicit forecasts of winter precipitation using an improved bulk microphysics scheme. part i: Description and sensitivity analysis. *Monthly Weather Review*, 132(2):519–542.

Tompkins A.M, 2005: The parameterization of cloud cover. *ECMWF Technical Memoranda*.

Wang Z., C.B. Schaaf, A.H. Strahler, M.J. Chopping, M.O. Román, Y. Shuai, C.E. Woodcock, D.Y. Hollinger, D.R. Fitzjarrald, 2014: Evaluation of MODIS albedo product (MCD43A) over grassland, agriculture and forest surface types during dormant and

snow-covered periods. *Remote Sens. Environ.,* 140, pp. 60-77, 10.1016/j.rse.2013.08.025

World Meteorological Organization, 1986: A preliminary cloudless standard atmosphere for radiation computation. *WPC-112, TD-No. 24*, 53pp.

Xu, K.-M., and D. A. Randall, 1996: A semiempirical cloudiness parameterization for use in climate models. *J. Atmos. Sci.*, 53, 3084–3102.

Yang, F., K. Mitchell, Y. Hou, Y. Dai, X. Zeng, Z. Wang, and X. Liang, 2008: Dependence of land surface albedo on solar zenith angle: observations and model parameterizations. J*ournal of Applied Meteorology and Climatology.* No.11, Vol 47, 2963-2982

Yang, Z.-L., G.-Y. Niu, K. E. Mitchell, F. Chen, M. B. Ek, M. Barlage, L. Longuevergne, K. Manning, D. Niyogi, M. Tewari, and Y.-L. Xia 2011: The community Noah land surface model with multiparameterization options (Noah-MP): 2. Evaluation over global river basins, *J. Geophys. Res.*, 116, D12110, doi:10.1029/2010JD015140.

Zdunkowski, W. G., Welch, R. M. and Korb, G. 1980: An investigation of the structure of typical two-stream methods for the calculation of solar fluxes and heating rates in clouds. *Beitr. Phys. Atmos.*, 53, 147–166.

Zhao, W.; Peng, Y.; Wang, B.; Li, J. 2018: Cloud Longwave Scattering Effect and Its Impact on Climate Simulation. *Atmosphere 9*, 153.